République Algérienne Démocratique et Populaire
Ministère de l'Enseignement Supérieur et de la Recherche Scientifique
Ecole Nationale polytechnique
Département génie des procédes et environement

المدرسة الوطنية المتعددة التقنيات
Ecole Nationale Polytechnique

LABORATOIRE DES SCIENCES ET TECHNIQUES DE L'ENVIRONNEMENT

End-of-Study Project

to obtain the State Engineer Diploma in Environmental Engineering
Process Engineering and Environment Option

Development and Characterization of PANI/GO/ZnO Supercapacitor Electrodes using Electrodeposition

Presented by:

HAMMA Abdelkrim

Under the supervision of: **Dr. DJELLOULI Naima**

Miss BOUAOUD Fatima

Presented and publicly supported on July, 11th, 2024

Against the Jury compound of:

President:	Dr. BENSADALLAH Leila	NPS, Algeria
Supervisor:	Dr. DJELLOULI Naima	NPS, Algeria
	Miss BOUAOUD Fatima	NPS, Algeria
Examiner:	Mr. KHERAT Mohamed	NPS, Algeria
Guest:	Dr. BOUSBAI M'hamed	TISC/ NPS, Algeria

République Algérienne Démocratique et Populaire
Ministère de l'Enseignement Supérieur et de la Recherche Scientifique
Ecole Nationale polytechnique
Département génie des procédes et environement

End-of-Study Project

to obtain the State Engineer Diploma in Environmental Engineering

Process Engineering and Environment Option

Development and Characterization of PANI/GO/ZnO Supercapacitor Electrodes using Electrodeposition

Presented by:

HAMMA Abdelkrim

Under the supervision of: **Dr. DJELLOULI Naima**

Miss BOUAOUD Fatima

Presented and publicly supported on July, 11th, 2024

Against the Jury compound of:

President:	Dr. BENSADALLAH Leila	NPS, Algeria
Supervisor:	Dr. DJELLOULI Naima	NPS, Algeria
	Miss BOUAOUD Fatima	NPS, Algeria
Examiner:	Mr. KHERAT Mohamed	NPS, Algeria
Guest:	Dr. BOUSBAI M'hamed	TISC/ NPS, Algeria

République Algérienne Démocratique et Populaire

Ministère de l'Enseignement Supérieur et de la Recherche Scientifique

Ecole Nationale polytechnique

Département génie des procédes et environement

Projet de fin d'études

Pour l'obtention du diplôme d'Ingénieur d'État en genie des procedes et environement

Développement et Caractérisation des Électrodes de Supercondensateurs PANI/GO/ZnO utilisant la Technique d'Électrodéposition

Présenté par:

HAMMA Abdelkrim

Sous la supervision de: **Dr. DJELLOULI Naima**

Mademoiselle BOUAOUD Fatima

Présenté et soutenu publiquement le 11 juillet 2024

Devant le jury composé de:

Présidente :	Dr. BENSADALLAH Leila	ENP, Algérie
Superviseur :	Dr. DJELLOULI Naima	ENP, Algérie
	Miss BOUAOUD Fatima	ENP, Algérie
Examinateur :	Mr. KHERAT Mohamed	ENP, Algérie
Invité:	Dr. BOUSBAI M'hamed	TISC/ ENP, Algérie

الملخص

تبحث هذه الدراسة في تطوير وتوصيف أقطاب مركبة من PANI/GO/ZnO للمكثفات الفائقة باستخدام تقنيات الترسيب الكهربائي. تم تخليق وتقييم عينات منPANI ، PANI/GO، PANI/ZnO، وPANI/GO/ZnOتم تقييم الأداء الكهروكيميائي باستخدام الفولطية الدوريةCV، الشحن والتفريغ الجلفاني الثابتGCD ، والتحليل الطيفي للمقاومة الكهروكيميائية EIS .تم إجراء التحليلات الهيكلية باستخدام المجهر الإلكتروني الماسح SEM والحيود بالأشعة السينية XRD. تظهر النتائج أن المركبات PANI/GO/ZnO تقدم أداءً كهروكيميائيًا محسّنًا بكفاءة تبلغ 139%، وطاقة تبلغ 9.8 واط ساعي/كجم، وسعة نوعية تبلغ 359 فاراد/جم، وزمن تفريغ يبلغ 209.8 ثانية .توفر هذه النتائج رؤى حول تحسين معايير الترسيب الكهربائي لتعزيز كفاءة المكثفات الفائقة.

الكلمات المفتاحية: مكثفات فائقة، PANI، أكسيد الجرافين، ZnO، الترسيب الكهربائي، الشحن والتفريغ الجلفاني الثابتGCD ، التحليل الطيفي للمقاومة الكهروكيميائية EIS .

Résumé

Cette étude examine le développement et la caractérisation des électrodes composites PANI/GO/ZnO pour supercondensateurs en utilisant des techniques d'électrodéposition. Des échantillons de PANI,PANI/GO, PANI/ZnO, PANI/GO/ZnO ont été synthétisés et évalués. La performance électrochimique a été évaluée en utilisant la voltammétrie cyclique (CV), la charge-décharge galvanostatique (GCD) et la spectroscopie d'impédance électrochimique (EIS). Les analyses structurelles ont été effectuées avec la microscopie électronique à balayage (SEM) et la diffraction des rayons X (XRD). Les résultats montrent que les composites PANI/GO/ZnO offrent une performance électrochimique améliorée avec une efficacité de 139 %, une énergie de 9,8 Wh/kg, une capacitance spécifique de 359 F/g et un temps de décharge de 209,8 secondes.

Ces résultats fournissent des informations pour optimiser les paramètres d'électrodéposition afin d'améliorer l'efficacité des supercondensateurs.

Mots-clés : Supercondensateurs, PANI, Oxyde de Graphène, ZnO, Électrodéposition, Charge-Décharge Galvanostatique (GCD), Spectroscopie d'Impédance Électrochimique (EIS).

Abstract

This study examines the development and characterization of PANI/GO/ZnO composite electrodes for supercapacitors using electrodeposition techniques. Samples of PANI, PANI/GO, PANI/ZnO, PANI/GO/ZnO were synthesized and evaluated. Electrochemical performance was assessed using cyclic voltammetry (CV), galvanostatic charge-discharge (GCD), and electrochemical impedance spectroscopy (EIS). Structural analyses were conducted with Scanning Electron Microscopy (SEM) and X-ray Diffraction (XRD). Results show that PANI/GO/ZnO composites offer improved electrochemical performance with an efficiency of 139 %, an energy of 9.8 Wh/kg,specific capacitance of 359 F/g and a discharge time of 209.8 secondes.

These results provide insights for optimizing electrodeposition parameters to enhance supercapacitor efficiency.

Keywords: Supercapacitors, PANI, Graphene Oxide, ZnO, Electrodeposition, Galvanostatic Charge-Discharge (GCD), Electrochemical Impedance Spectroscopy (EIS).

Acknowledgement

First and foremost, I would like to thank God Almighty for granting me the courage, strength, and determination to complete this modest work.

I would like to extend my heartfelt thanks to Ms. DJELLOULI Naima for her unwavering support and guidance throughout the preparation of this thesis. Your mentorship has been invaluable.

I also express my gratitude to Ms. BOUAOUD Fatima for her assistance and kindness. Your help has been greatly appreciated.

I would like to warmly thank Mr. BOUSBAI M'Hamed, representant of the Technology and Innovation Support Center at The National Polytechnic School.

I am also grateful to Mrs BENSADALLAH Leila. for agreeing to chair the jury of my defense.

My sincere thanks go to Mr. KHERAT Mohamed for his keen interest in my project and for agreeing to examine it and be a member of the jury.

I also thank Mr. NAITBOUDA Abdelyamineand and OULD HAMOU Malek for thier help and assistance .

Lastly, I would like to thank all the teachers who have helped me and contributed to my education throughout my studies. Your dedication and support have shaped my academic journey.

This version maintains the original content and acknowledges everyone who contributed to your work.

Dedication

To my dear parents, my loving family, and my precious friends,

This dedication is for you, to tell you how important you are to me. You are the strength that pushes me forward, the smile that brightens my darkest days, and the safe haven in the turmoil of life.

To my parents, thank you for giving me life, education, and unconditional love. You are my first teachers and the guardians of my dreams. You have laid the foundations upon which I build my life, and for that, I will be eternally grateful.

To my family, thank you for being my anchor and my guiding light. Each of you, in your unique way, has contributed to shaping the person I am today. You are the link that connects me to the past while accompanying me toward the future.

And to my friends, thank you for being there for me in moments of joy and in moments of challenge. You are the brothers and sisters I have chosen, the companions on this journey of life.

I dedicate every victory, every achievement, and every moment of happiness to you all. Your support, your love, and your friendship are the greatest gifts I could ever ask for. Together, we face whatever comes our way, and I am convinced that the best is yet to come.

With all my gratitude and love,

Table of contents

Figures table

Tables list

List of abbreviations

Ag/AgCl: Silver/Silver Chloride Electrode
CV: Cyclic Voltammetry
EDS: Energy Dispersive X-Ray Spectroscopy
EIS: Electrochemical Impedance Spectroscopy
GCD: Galvanostatic Charge-Discharge
GO: Graphene Oxide
GRAS: Generally Recognized As Safe
ITO: Indium Tin Oxide
NPs: Nanoparticles
PANI: Polyaniline
PEG: Polyethylene Glycol
SEM: Scanning Electron Microscopy
SS: Stainless Steel
XRD: X-Ray Diffraction
ZnO: Zinc Oxide
Cs: specific capacitance

General introduction

In the realm of energy storage solutions, supercapacitors have emerged as promising devices due to their rapid charge-discharge cycles and high power density compared to conventional batteries . Supercapacitors are utilized in various domains, including renewable energy systems, electric vehicles, portable electronics, and industrial power backup systems. Their ability to deliver quick bursts of energy makes them essential in applications requiring high power output and efficiency . The importance of supercapacitors lies in their potential to complement or even replace batteries in certain applications, enhancing energy storage capabilities and contributing to the development of more efficient and sustainable energy systems[1].

Among the various materials and methods explored for enhancing supercapacitor performance, the combination of a conductive polymer: the Polyaniline (PANI), Graphene Oxide (GO), and Zinc Oxide (ZnO) stands out for its interesting synergistic properties [2].

Supercapacitors operate on the principles of electrostatic double-layer capacitance and electrochemical pseudocapacitance. The incorporation of PANI, a conducting polymer, along with GO, known for its high surface area and excellent conductivity, and ZnO, recognized for its electrochemical stability, aims to enhance the overall performance of supercapacitors [2]. The electrodeposition technique, which is a versatile method for fabricating thin films and coatings, is employed to synthesize these composite electrodes with controlled morphology and composition [3].

This work focuses on the development and characterization of PANI/GO/ZnO supercapacitor electrodes using electrodeposition techniques. The primary objective of this study is to investigate the electrochemical performance of PANI/GO/ZnO composite electrodes. By varying the electrodeposition parameters, we aim to optimize the material properties for improved capacitance, energy density, and cycle stability. The research includes comprehensive electrochemical characterization using techniques such as cyclic voltammetry (CV), galvanostatic charge-discharge (GCD), and electrochemical impedance spectroscopy (EIS), alongside surface and structural analyses using Scanning Electron Microscopy (SEM) and X-ray Diffraction (XRD).

The research is structured as follows:

Chapter 1: Theoretical Background : This chapter provides an overview of supercapacitor fundamentals, including the types, components, and working principles. It also discusses the properties and benefits of PANI, GO, and ZnO as electrode materials and the basics of the electrodeposition process.

Chapter 2: Materials and Experimental Techniques : This chapter details the materials used in the study, including the preparation and characterization of PANI, GO, and ZnO. It describes the

electrodeposition process for fabricating the composite electrodes and the various experimental techniques used for their electrochemical and structural characterization.

Chapter 3: Results and Discussion : This chapter presents the findings from the electrochemical tests and surface analyses. It discusses how different electrodeposition parameters can influence the microstructure and electrochemical performances of the PANI/GO/ZnO electrodes. The results are then analyzed to identify the optimal conditions for achieving high-performance supercapacitor electrodes.

This structured approach aims to contribute to the existing knowledge on supercapacitors by providing a detailed analysis of the effects of electrodeposition parameters on the performance of PANI/GO/ZnO composite electrodes. The insights gained from this research will be valuable for industries relying on advanced energy storage solutions, helping to optimize supercapacitor design and enhance their practical applications.

Chapter 1 :Literature review

1.1 Historical Context

Electrostatic and electrolytic capacitors are considered first and second-generation capacitors. These early capacitors were developed to be used as primary circuit elements for holding direct current charges at the microfarad level or for filtering frequencies in alternating current circuits [47]. With the rapid evolution of materials, the third generation, known as the supercapacitor, was invented. [47, 48]. Although the idea that charges could accumulate on solids was known since antiquity (the Greek word for amber, 'elektron,' dates back to the Greek era), the first patent for an electrochemical capacitor was only filed in 1957 by General Electric [49, 50]. This capacitor consisted of porous carbon electrodes utilizing the double-layer capacitance mechanism for charge. With other modifications, the first practical supercapacitor was developed by SOHIO (Standard Oil of Ohio) using a carbon paste soaked in an electrolyte as described in a 1970 patent. In 1978, NEC (Nippon Electric Company) eventually introduced (under license from SOHIO) the first capacitors under the name "supercapacitor," and its application was used to provide backup power for computer memory retention [49].

The rapid growth of mobile electronics and alternative energy vehicles created a need for advanced electrochemical energy storage devices with high power capacities. This need led to substantial research and development of supercapacitors. In the early 1990s, the United States Department of Energy (DOE) strongly advocated for funding research on batteries and supercapacitors to raise international awareness of the potential of supercapacitors. Since then, supercapacitors have evolved through several generations of designs based on the development of electrode materials, composites, hybridization, and appropriate electrolytes to improve performance and reduce costs [51].

Significant efforts have been dedicated to the research and development of supercapacitors to improve performance, particularly by increasing their energy density. To this end, more advanced supercapacitors, called pseudo-capacitors, have been developed, in which the electroactive materials are composed of carbon particles to form composite electrode materials. The electrochemical reaction of the electroactive material in a pseudo-capacitor occurs at the interface between the electrode and the electrolyte through mechanisms of adsorption, intercalation, or redox (reduction-oxidation) [47]. In this way, the capacitance of the electrode and energy density can be significantly increased.

1.2 Definition of supercapacitor:

A supercapacitor is an electrochemical energy storage device that stands out for its ability to offer rapid charge and discharge cycles compared to conventional batteries. It operates on the principle of storing energy through the formation of an electrostatic double-layer and/or through electrochemical pseudo-capacitance. The core components of a supercapacitor include electrodes made from materials with high surface areas such as activated carbon, metal oxides, or conducting polymers, an electrolyte that facilitates ion transport between electrodes, and a separator that prevents electrical contact between the electrodes while allowing ionic movement.

Supercapacitors are characterized by their high-power density, which allows them to release and absorb energy quickly, and their ability to endure hundreds of thousands of charge and discharge cycles without significant degradation in performance. These attributes make supercapacitors ideal for applications requiring quick energy bursts and high power efficiency, such as in regenerative braking systems in electric vehicles, power stabilization in renewable energy systems, and in providing peak power supply in electronic devices[4].

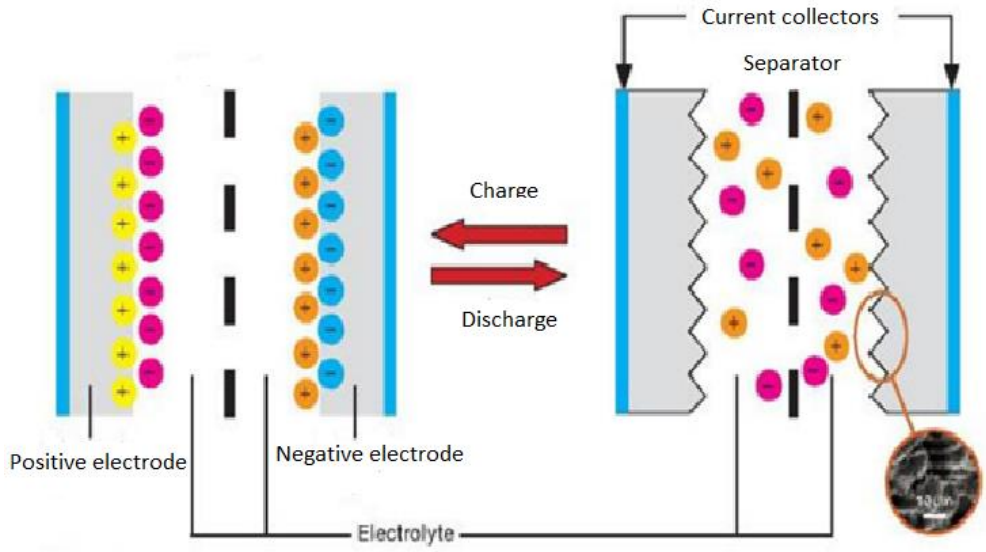

Figure 1: Composition and work principle of a supercapacitor (CNRS Éditions).

1.3 Types of supercapacitors:

The basics of supercapacitors have been examined and discussed in many reviews. The term "supercapacitor" generally refers to various types of electrochemical capacitors. Therefore, it is extremely important to use the correct terminology to distinguish between the different types. As briefly mentioned above, a distinction is made between EDLCs, pseudo-capacitors, and hybrid capacitors. The differences between these types are primarily based on the nature of the active material used for the electrodes and the mode of energy storage within these materials (Fig. 2) [52].

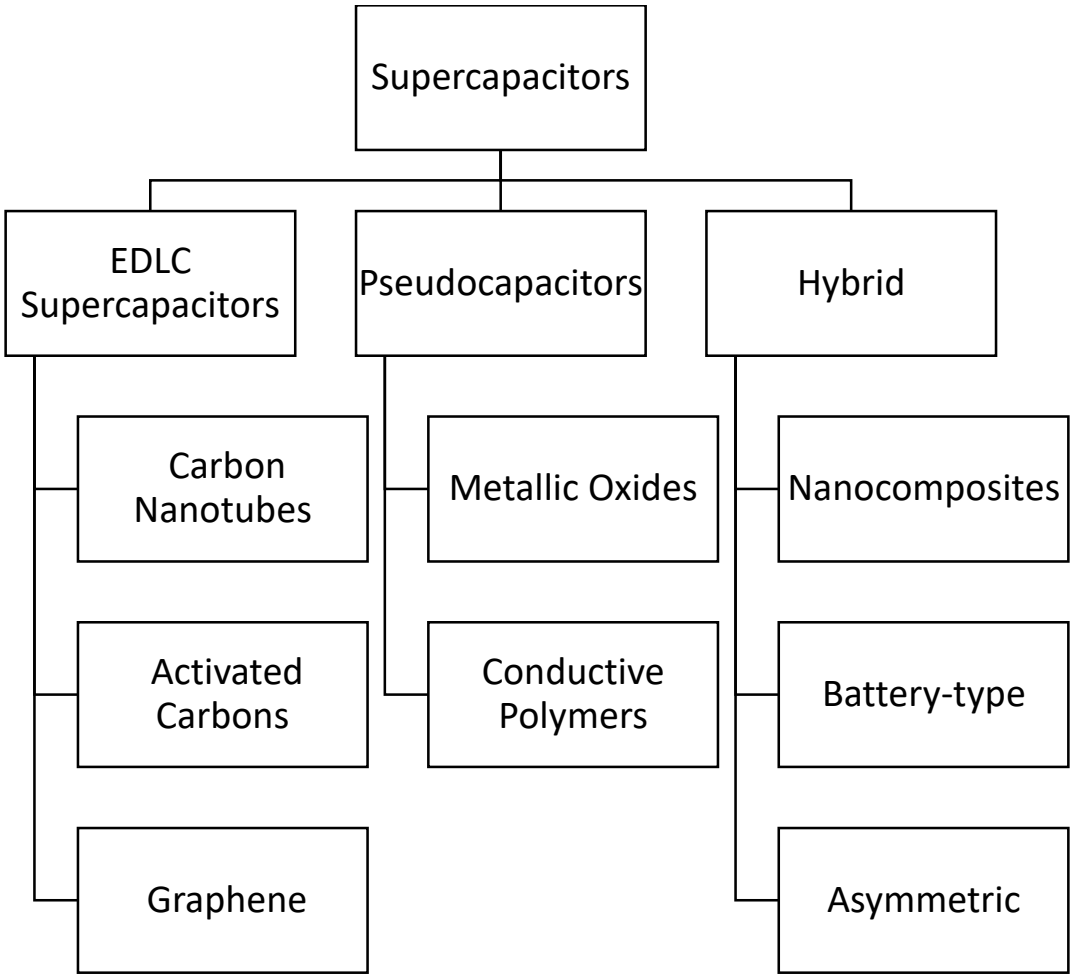

Figure 2 : Different types of supercapacitors [52].

1.3.1 Electrostatic Double-Layer Capacitance (EDLC):

Electrochemical Double-Layer Capacitors (EDLCs) function based on the electrostatic attraction between two layers of opposite charges at the electrode-electrolyte interface. Upon applying a voltage, ions in the electrolyte move towards the electrode surface, forming an electric double layer that acts as a capacitor, thus storing electrical energy. The process involves three stages: charging, where ions migrate to the electrode surface forming the double layer; storage, where the double layer holds the electrical energy, with the storage capacity influenced by the electrode surface area, ionic conductivity of the electrolyte, and the applied voltage; and discharging, where the stored energy is released as the ions migrate back into the electrolyte when the supercapacitor is connected to a load[5].

1.3.2 Electrochemical Pseudo-capacitance EPC:

Electrochemical Pseudo-capacitor (EPC) supercapacitors operate based on both electrochemical reactions and the formation of an electric double layer at the electrode-electrolyte interface. When a voltage is applied, ions in the electrolyte migrate to the electrode surface, forming an electric double layer and facilitating electrochemical reactions that involve electron transfer between the electrode and the electrolyte. This process, known as pseudo-capacitance, can be divided into three stages: charging, where ions migrate to the electrode surface forming the double layer and electrochemical reactions occur; storage, where the combined effect of the double layer and electrochemical reactions store electrical energy, influenced by electrode surface area, ionic conductivity, and applied voltage; and discharging, where the ions migrate back into the electrolyte and the electrochemical reactions are reversed, releasing stored energy and electrons back into the circuit [5].

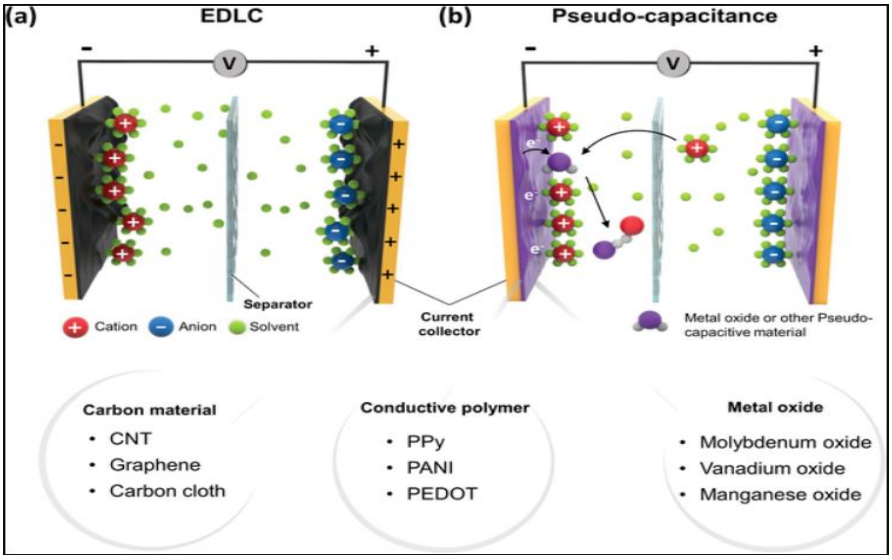

Figure 3: Energy storage mechanisms for EDLC (a) and pseudo-capacitance (b) devices, and commonly used electrode materials for corresponding mechanisms [6].

1.4 Components of supercapacitor:

1.4.1 Electrodes:

Electrodes in supercapacitors are crucial components that determine the device's performance. They must have good electrical conductivity, high chemical stability, and a well-designed pore structure to store and release energy efficiently. The use of porous materials with suitable pore sizes improves the storage capacity and overall performance by allowing more ions from the electrolyte to interact with the electrode surface. Additionally, these electrodes should be cost-effective, environmentally friendly, and capable of withstanding various operating conditions.

1.4.1.1 Materials for Supercapacitor Electrodes:

Carbon-Based Materials: Recent progress highlights the extensive use of carbon-based materials, such as activated carbon, carbon nanotubes, graphene, and carbon nanofibers, for

supercapacitor electrodes. These materials are favored for their high surface area, excellent electrical conductivity, and chemical stability, which contribute to high capacitance and energy density [7].

Metal Oxides and Sulfides: Electrospun nanomaterials, including metal oxides (e.g., MnO2, RuO2) and metal sulfides, have been explored for their pseudocapacitive properties, offering higher specific capacitance than carbon materials. The electrospinning technique allows for the creation of one-dimensional (1D) nanostructures with controlled dimensions and high surface area, enhancing the electrochemical performance of supercapacitor electrodes [8].

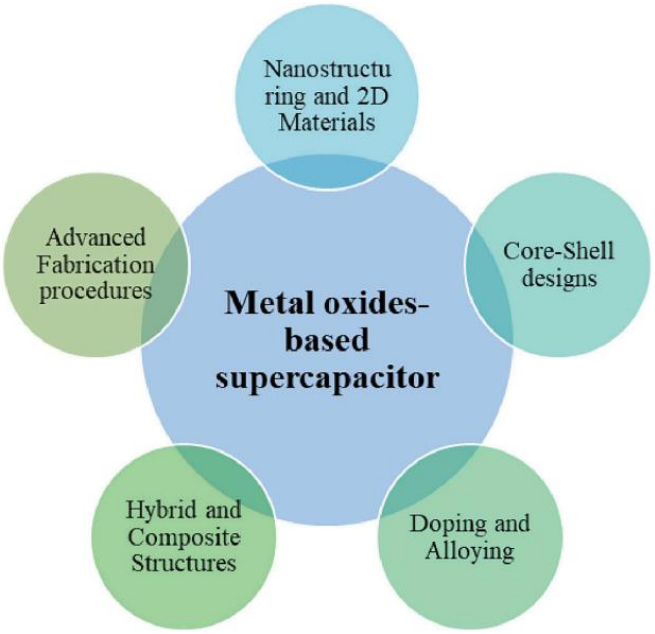

Figure 4:Recent development made in the fabrication of metal-based electrodes [1].

Conducting Polymers: Polyaniline, polypyrrole, and polythiophene are examples of conducting polymers which are another pseudocapacitive electrode material that has been widely studied due to its relatively high capacity, high energy density, adjustable redox activity by chemical modification, good conductivity in doped states, wide voltage windows, as well as easy production, low environmental impact, and low cost. They are capable of storing charge in their volume, as no structural change such as phase changes occurs during the charge/discharge mechanism. Due to this, conducting polymers can offer superior capacitance due to their more extensive surfaces and redox storage capabilities [9].

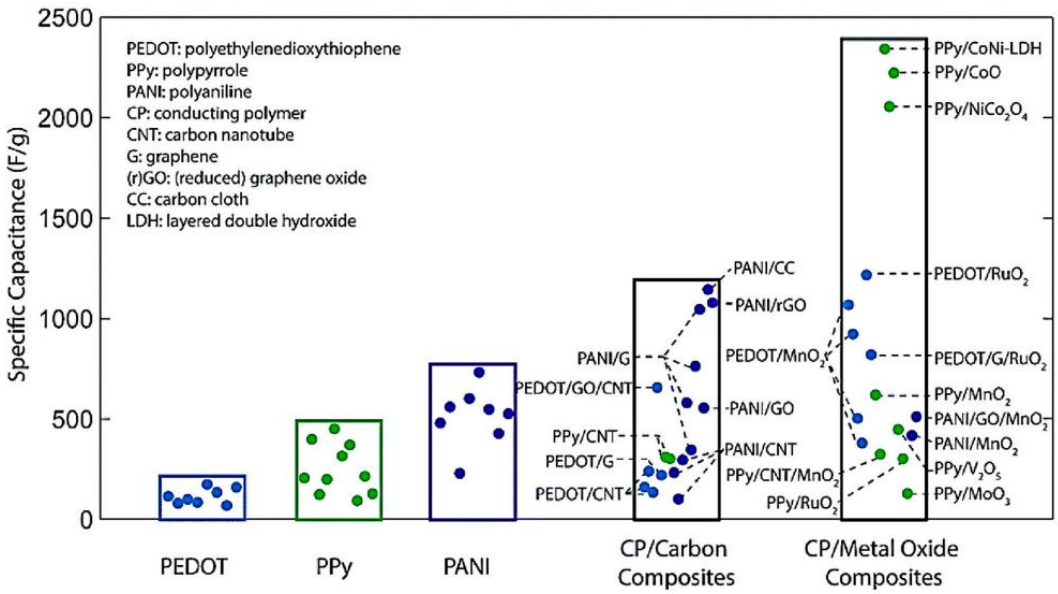

Figure 5: Comparison of the Cs of CPs based supercapacitors [1].

1.4.2 Electrolyte:

The electrolyte is an ion-conducting liquid that allows the transport of electrical charges between the two plates of the supercapacitor. The charges depicted represent the electrolyte's ions. Electrolytes have a very great importance concerning the performance of supercapacitors; a quality electrolyte can offer a wide voltage range, high electrochemical stability, high ionic concentration and conductivity, low viscosity, and low toxicity [5]. And the main electrolytes currently used for supercapacitors are listed in Table 1.

Table 1:The main electrolytes used for supercapacitors.[10]

Type	**Chemical Composition (most common)**	**Ionic Conductivity**	**Electrochemical Stability**	**Safety**	**Cost**
Organic electrolytes	Salts in organic solvents (e.g., $LiPF_6$ in carbonates or ethers)	Moderately high	Moderately high	Flammable (commonly) and may leak	Moderate
Ionic liquid electrolytes	Organic cations (e.g., imidazolium) with inorganic/organic anions (e.g., BF_4^-).	Moderate	Moderately high-to-high	Combustible at elevated T and may leak	Moderately high

Aqueous electrolytes	Inorganic salts or acids in water (e.g., NaCl, KOH, H_2SO_4).	Highest	Smallest	Nonflammable but may leak	Lowest
Solid polymer electrolytes	Salts in polymer matrices (e.g., PEO, PAN).	Lowest (commonly)	Moderate-to-high	Combustible at elevated T	Moderately high, some are expensive to incorporate
Inorganic solid electrolytes	Oxides, sulfides, and other inorganic compounds (e.g., garnets, LiPON)	Low-to-Moderate	Moderate-to-high	Nonflammable, some may be toxic	Moderate-to-high, expensive to incorporate

1.4.3 Separator:

This component is crucial as it prevents the physical contact between the electrodes (which would lead to a short circuit), while allowing the free movement of ions. It is typically made from a porous, non-conductive material like polypropylene or polyethylene.

1.4.4 Current Collectors:

These are conductive materials that connect the electrodes of the supercapacitor to the external circuit. They must be highly conductive to efficiently transfer electrons in and out of the supercapacitor.

1.5 PANI:

1.5.1 Definition of Polyaniline (PANI):

Polyaniline (PANI) is a conducting polymer of the semi-flexible rod polymer family. It is known for its ease of synthesis and its wide range of applications due to its electrical properties and stability. PANI can exist in various oxidation states (Figure 6), each providing different levels of conductivity. The most common forms are the leucoemeraldine (fully reduced), emeraldine (half-oxidized), and pernigraniline (fully oxidized) bases, with the emeraldine salt form being the most conductive when protonated.

PANI's conductivity can be tuned through doping processes, where the conductivity changes significantly with the oxidation state and the nature of the dopant used. This makes it highly versatile for various electronic and electrochemical applications [11].

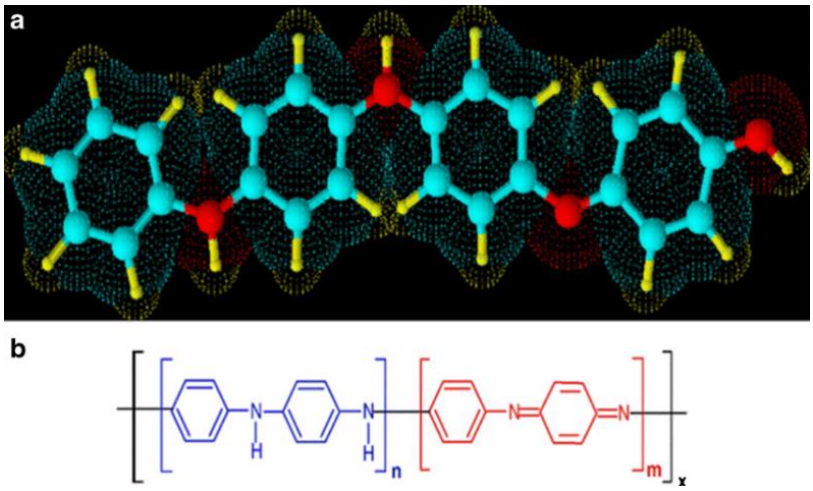

Figure 6: (a) 3D structure of polyaniline. The carbon atoms (cyan balls), nitrogen atoms (red balls), hydrogen atoms (small yellow balls), and clouds (molecular orbitals). (b) Polyaniline 2D structure.

1.5.2 Synthesis of PANI:

1.5.2.1 Chemical Oxidation Synthesis of Polyaniline (PANI):

The chemical oxidation synthesis of polyaniline (PANI) involves the oxidative polymerization of aniline monomers using an oxidizing agent in an acidic medium, a method valued for its simplicity and effectiveness. Aniline is dissolved in an acidic solution, such as hydrochloric acid (HCl), ensuring the monomer remains protonated. Ammonium persulfate (APS) is commonly used as the oxidizing agent, added to the aniline solution to initiate polymerization. This reaction forms radical cations that couple to create the PANI chain, linking aniline units through their nitrogen atoms. The reaction continues until the desired molecular weight and conductivity are reached, after which the polymer is filtered, washed, and dried. The synthesized PANI is often doped with a protonic acid to enhance its conductivity, increasing the density of charge carriers within the polymer[12].

1.5.2.2 Electrochemical synthesis:

The electrochemical synthesis of polyaniline (PANI) involves the electro-polymerization of aniline on an electrode surface within an electrochemical cell, allowing precise control over the polymer film's thickness and morphology. This process begins with setting up an electrochemical cell featuring an anode and cathode, often made of conductive materials like platinum or glassy carbon. Aniline is dissolved in an acidic electrolyte solution, which is then used in the cell. Upon applying a voltage, aniline monomers at the anode oxidize to form radical cations that undergo reactions to create PANI chains on the electrode surface. The polymer film grows as the reaction continues, with its characteristics adjustable through reaction conditions such as voltage and time. Post-synthesis, the PANI can be doped to enhance its electrical properties [13].

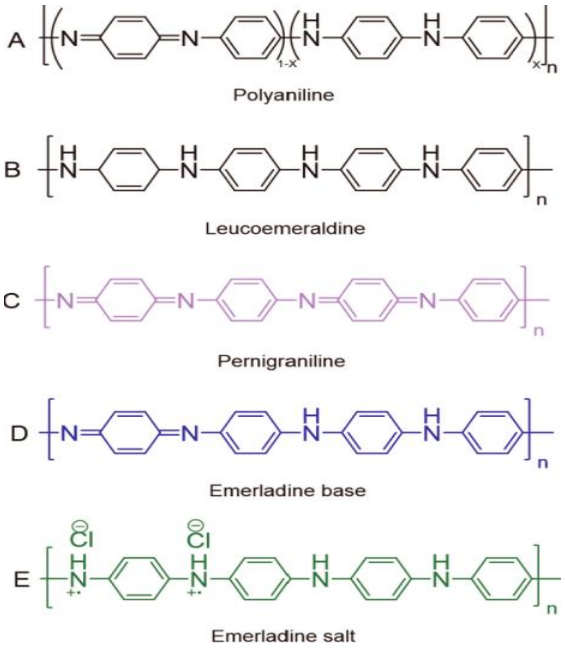

Figure 7: Chemical structures of the different forms of polyaniline (PANI): (A) polyaniline, (B) leucoemeradine, (C) pernigraniline, (D) emeraldine base (EB), and (E) emeraldine salt (ES), [14].

1.6 Graphene Oxide

1.6.1 Definition of Graphene Oxide:

Graphene oxide (GO) is a type of graphene that has been oxidized to introduce oxygen-containing functional groups, such as hydroxyl, carboxyl, and epoxy groups, onto its surface. This oxidation process can be achieved through various methods, including chemical oxidation, electrochemical oxidation, and mechanical exfoliation. GO is a highly reactive and hydrophilic material that can be easily dispersed in water and other polar solvents [15].

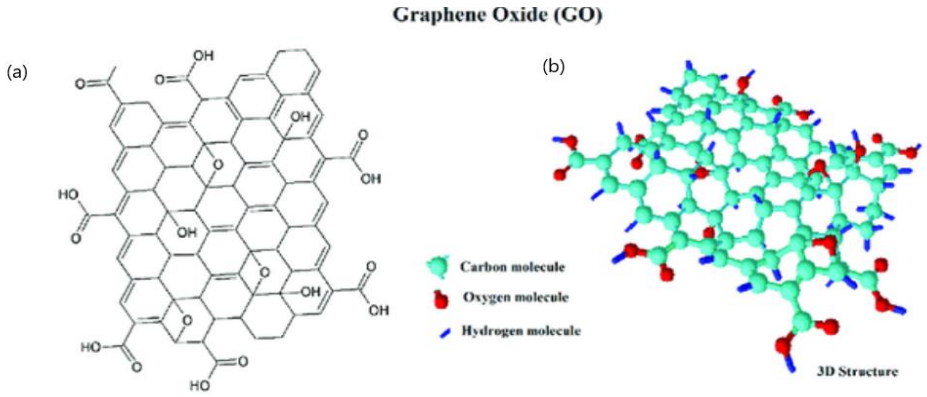

Figure 8:The structure of Graphene Oxide (GO),(a) 2D structure (b) 3D structure [16].

1.6.2 Synthesis of Graphene Oxide:

1.6.2.1 Chemical oxidation:

Chemical oxidation is a method of synthesizing graphene oxide (GO) by reacting graphite with a strong oxidizing agent, such as potassium permanganate ($KMnO_4$) or sulfuric acid (H_2SO_4), in the presence of a catalyst, such as sodium nitrate ($NaNO_3$) or potassium nitrate (KNO_3). This method is also known as the Hummers' method [17,18].

1.6.2.2 Electrochemical oxidation:

Electrochemical oxidation is a method of synthesizing graphene oxide (GO) by reacting graphite with an oxidizing agent, such as potassium permanganate ($KMnO_4$) or sulfuric acid (H_2SO), in an electrochemical cell. This method is also known as electrochemical exfoliation [19].

1.6.2.3 Mechanical exfoliation:

Mechanical exfoliation is a method of synthesizing graphene oxide (GO) by mechanically exfoliating graphite using a mechanical process, such as sonication or ball milling. This method is also known as mechanical exfoliation [20].

1.7 Zinc Oxide:

1.7.1 Definition of ZnO:

Zinc Oxide Nanoparticles (ZnO NPs) are nanoscale particles of zinc oxide that typically have diameters less than 100 nanometers. They are known for their unique physical and chemical properties, such as UV absorption, catalytic activity, and large surface area relative to their size [21]. ZnO NPs are considered less toxic and more biocompatible than other metal oxide nanoparticles like TiO_2 and are recognized as safe (GRAS) by the FDA [22].

1.7.2 Synthesis methods:

1.7.2.1 Electrochemical synthesis:

The electrochemical synthesis of Zinc Oxide (ZnO) from a $ZnSO_4 \cdot 7H_2O$ solution involves reducing zinc ions to metallic zinc on a conductive substrate and subsequently oxidizing the zinc to form ZnO. This process is conducted in an electrochemical cell with a working electrode (e.g., glassy carbon, platinum, or ITO), a counter electrode (typically platinum or graphite), and a reference electrode (such as Ag/AgCl or SCE) in an aqueous $ZnSO_4 \cdot 7H_2O$ solution. The method allows precise control over the ZnO film's thickness, morphology, and particle size by adjusting deposition parameters. It produces high-purity, uniform ZnO essential for applications in sensors, photovoltaics, and supercapacitors, and is environmentally friendly and cost-effective [23].

1.7.2.2 Co-precipitation:

Co-precipitation is a straightforward and widely used method for synthesizing zinc oxide nanoparticles (ZnO NPs). In this process, a solution containing dissolved zinc ions (usually from a salt like zinc nitrate or zinc acetate) is mixed with a precipitating agent, such as sodium hydroxide or ammonium hydroxide. The addition of the precipitating agent causes the zinc ions to precipitate

out of the solution as zinc hydroxide. The zinc hydroxide precipitate is then collected, washed, and calcined (heated at high temperatures) to convert it into zinc oxide nanoparticles. By controlling various parameters such as the concentration of reactants, pH, temperature, and reaction time, the size, morphology, and other properties of the resulting ZnO NPs can be tuned. The co-precipitation method offers several advantages, including its simplicity, low cost, and the ability to produce large quantities of nanoparticles. However, achieving uniform particle size and morphology can be challenging, and additional techniques may be required to obtain more monodisperse nanoparticles [24].

1.7.2.3 The sol-gel method:

The sol-gel method is a versatile and widely used technique for synthesizing zinc oxide nanoparticles (ZnO NPs). In this process, a sol (colloidal solution) containing zinc precursors, such as zinc acetate or zinc nitrate, is prepared by dissolving the precursor in a suitable solvent, typically an alcohol like ethanol or isopropanol. A gelling agent, such as polyethylene glycol (PEG) or citric acid, is then added to the sol to promote the formation of a gel network. The sol-gel transition occurs through hydrolysis and condensation reactions, leading to the formation of a three-dimensional network of zinc oxide. The gel is then dried to remove the solvent, resulting in a xerogel. Finally, the xerogel is calcined (heated) at high temperatures, typically between 300° C and 800°C, to remove any organic residues and crystallize the zinc oxide nanoparticles. By controlling various parameters such as the choice of precursors, solvent, gelling agent, pH, and calcination temperature, the size, morphology, and properties of the resulting ZnO NPs can be tuned. The sol-gel method offers several advantages, including low processing temperatures, high purity, homogeneity, and the ability to produce nanoparticles with controlled size and shape [25].

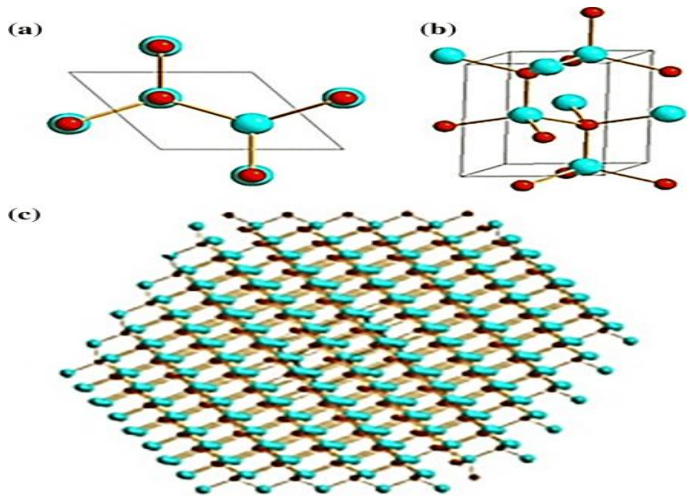

Figure 9:The crystal structure of ZnO unit cell based on Rietveld refinement a 2D view, b 3D vied, c 3D view of poly atomic ZnO (Blue ball = Zn atoms (bigger in size) and red ball = oxygen atoms), [26].

1.8 Electrochemical performance of supercapacitors:

1.8.1 Voltage dependent capacitance:

The capacitance of supercapacitors is not constant but varies with the voltage applied across its terminals. This voltage-dependent capacitance is an important characteristic that must be considered when using supercapacitors as part of an energy supply system. The voltage difference over the whole range is between 15% and 20% of the rated capacity, which cannot be ignored in most designs [27]. While the traditional capacitance C is defined as the ratio of stored charge q to voltage V (C = q/V), for supercapacitors the differential capacitance Cdiff is a more relevant measure. Cdiff is defined as the ratio of the change in stored charge dq to the change in voltage dV that caused it

$$(Cdiff = dq/dV = idt/dV)\text{[28]} \quad (01)$$

In summary, the voltage-dependent capacitance is a key electrical characteristic of supercapacitors that influences their performance in energy storage systems. The differential capacitance Cdiff provides a more accurate description of this behavior compared to the traditional capacitance C.

1.8.2 The Equivalent Series Resistance (ESR):

The Equivalent Series Resistance (ESR) in supercapacitors is a crucial parameter that affects the performance and efficiency of these devices. ESR is the total resistance of a supercapacitor, including the internal resistance of the electrodes, the electrolyte, and the connections. It is measured in ohms (Ω) and represents the opposition to the flow of current through the supercapacitor [29].

The ESR of a supercapacitor is influenced by several factors, including the type and quality of the electrodes, the electrolyte used, and the design of the supercapacitor itself. In general, a lower ESR is desirable, as it allows for faster charging and discharging of the supercapacitor, as well as higher power density and efficiency [30].

1.8.3 Energy density:

Energy density is a crucial parameter for evaluating supercapacitors, determining the amount of energy stored per unit volume or mass, typically expressed in watt-hours per kilogram (Wh/kg) or watt-hours per liter (Wh/L). It is calculated using the formula

$$(E = \frac{1}{2}CV^2) \quad (02)$$

where (C) is the capacitance and (V) is the operating voltage. Higher energy density means more energy storage, essential for applications like electric vehicles and portable electronics. Factors affecting energy density include the electrode material and structure, and the type and stability of the electrolyte. Enhancing energy density involves developing advanced electrode materials with high surface areas, optimizing electrolytes for higher operating voltages, and improving electrode design for better ion transport. While supercapacitors typically have lower energy density than

batteries, they offer high power density and long cycle life, making them ideal for applications requiring rapid energy delivery and durability.

1.9 Electrodeposition:

1.9.1 Definition:

Electrodeposition is a versatile process used to form a coherent metal coating on an electrically conductive surface through controlled electrolytic reduction of metal ions or the oxidation of polymers in solution. This technique involves an electrochemical cell with two electrodes immersed in an electrolyte solution containing metal ions or the polymer solution. The object to be plated serves as the cathode, where metal ions are reduced and deposited, while the anode, usually made of the deposition metal, either dissolves or facilitates an oxidation reaction to balance the charge. Applying a voltage across the electrodes drives the metal ions to the cathode, where they gain electrons and form a solid metal coating. The general cathode reaction is

$$M^{n+} + ne^{-} \rightarrow M$$

The process parameters, such as voltage, current density, electrolyte temperature, and metal ion concentration, can be adjusted to control the thickness and quality of the metal layer [31].

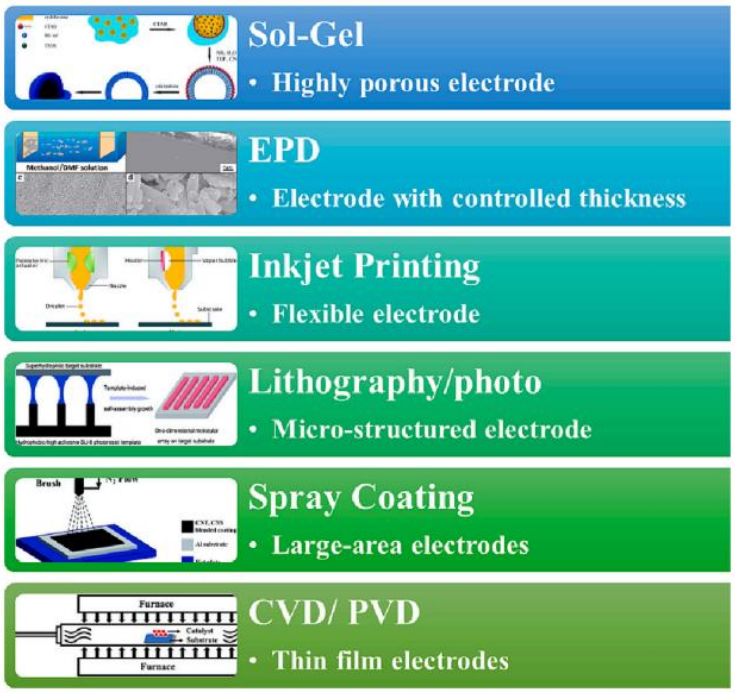

Figure 10: Different techniques for electrode fabrication.

1.9.2 Electrodeposition using Cyclic voltammetry (CV):

Electrodeposition using a three-electrode system in an electrochemical station through cyclic voltammetry (CV) offers precise control over metal deposition by monitoring and controlling the electrochemical environment. The system consists of a working electrode, counter electrode, and

reference electrode. The working electrode, where metal deposition occurs, is typically a conductive material like platinum, gold, or glassy carbon. The counter electrode, usually made of an inert material like platinum wire, completes the circuit and balances the current by facilitating oxidation reactions. The reference electrode, such as a Saturated Calomel Electrode (SCE) or Silver/Silver Chloride (Ag/AgCl) electrode, provides a stable potential for accurate measurements. In CV, the potential applied to the working electrode is swept linearly between two set values at a controlled scan rate, reaching potentials where metal ions in the solution reduce and deposit onto the electrode surface. The current response, plotted as a voltammogram, reveals peaks indicating oxidation or reduction reactions. Analyzing these curves helps determine the optimal potential range for efficient deposition, with cathodic peaks corresponding to metal ion reduction. Reversing the potential sweep allows the study of deposition reversibility by observing anodic peaks, which ideally mirror the cathodic peaks. This method enables real-time monitoring and optimization of deposition conditions by adjusting variables like scan rate, potential range, electrolyte composition, and temperature to achieve desired film thickness and morphology. Overall, the three-electrode system with CV provides high precision and control, making it ideal for creating high-quality metal coatings.

Electrodeposition is widely used for purposes such as providing corrosion resistance, enhancing appearance, increasing thickness of parts, or creating metal objects from scratch in applications ranging from electronics and decorative items to heavy machinery and aerospace components [31,32].

1.10 Electrochemical characterization:

1.10.1 Cyclic Voltammetry (CV):

Cyclic Voltammetry (CV) is a vital electrochemical technique used to evaluate the performance of supercapacitors by providing detailed information on their capacitive behavior, energy storage capability, and electrochemical stability. The basic setup involves a three-electrode system: the working electrode, which is the material being tested (e.g., GO/PANI/ZnO composite), the counter electrode, typically a platinum wire or graphite rod, and the reference electrode, such as Ag/AgCl or a saturated calomel electrode (SCE), which provides a stable reference potential. The cell is filled with an appropriate electrolyte solution (e.g., aqueous H_2SO_4 or KOH) to facilitate ion transport. An electrochemical workstation or potentiostat controls the potential applied to the working electrode and measures the resulting current.

The procedure starts with setting the working electrode potential to an initial value where no significant electrochemical reactions occur. The potential is then swept linearly to a set vertex potential (e.g., from 0 V to 0.8 V) and reversed back to the initial potential, often repeated several times. The scan rate, such as 10 mV/s, can be varied to study the kinetics of the electrochemical processes. During this sweep, the current resulting from the electrochemical reactions at the working electrode is recorded as a function of the applied potential.

In analyzing CV data, ideal capacitive behavior is indicated by nearly rectangular CV curves, showing a constant capacitive response over the potential range. Peak currents in the CV curve signify redox reactions, which are crucial for pseudocapacitive materials like PANI, where these peaks are associated with faradaic reactions. This method allows researchers to thoroughly assess the electrochemical characteristics and performance of supercapacitor electrodes [31,32].

Charge Calculation:

The charge stored in a supercapacitor can be calculated from a cyclic voltammetry (CV) plot by integrating the current with respect to time over a complete cycle. The CV plot displays current (I) versus applied potential (V). The area under the CV curve represents the total charge (Q) passed during the electrochemical processes, which is found by integrating the current (I) with respect to time (t). Since the potential sweep rate (ν) *is* (dV/dt), the integral with respect to potential can be used:

$$Q = \int_{t_0}^{t_1} I(t)dt = \int_{V_0}^{V_1} \frac{I(V)}{\nu} dV. \quad (03)$$

In practice, numerical integration techniques like the trapezoidal rule are applied to digitized CV data:

$$Q = \frac{1}{\nu} \sum_{i=0}^{n-1} \left(\frac{I(V_i) + I(V_{i+1})}{2} \right) (V_{i+1} - V_i). \quad (04)$$

This calculation provides the total charge stored or released, reflecting the capacitive and pseudocapacitive behavior of the supercapacitor's electrode material [32].

Reversibility and Stability:

The reversibility of the electrochemical reactions can be assessed by the symmetry of the forward and reverse scans. High reversibility indicates good electrochemical stability.

Long-term stability can be evaluated by repeating the CV cycles and observing any changes in the shape and area of the CV curves over many cycles.

1.10.1.1 Applications in Supercapacitor Evaluation:

Material Characterization: CV helps in characterizing the electrochemical properties of new electrode materials, such as GO/PANI/ZnO composites, by identifying their capacitive and pseudocapacitive behaviors.

Performance Comparison: By comparing the CV curves of different materials or composites, researchers can identify which materials offer better capacitive performance and stability.

Optimization: CV is used to optimize the synthesis and fabrication processes of supercapacitor electrodes by evaluating how different parameters (e.g., material composition, electrode thickness) affect electrochemical performance.

1.10.2 Galvanostatic Charge-Discharge (GCD):

Galvanostatic Charge-Discharge (GCD) is a crucial electrochemical technique used to assess supercapacitors by analyzing their charge-discharge behavior under constant current conditions, offering insights into specific capacitance, energy density, power density, and cycle stability. In a three-electrode system, the working electrode (e.g., GO/PANI/ZnO composite) is tested against a counter electrode (platinum or graphite) and a reference electrode (Ag/AgCl or SCE), while a two-electrode system uses symmetric electrodes. The cell is filled with an electrolyte like aqueous H_2SO_4 or KOH, and an electrochemical workstation controls the current and measures the voltage response. During GCD, a constant current charge the supercapacitor, increasing the potential linearly until a voltage limit is reached, then reverses to discharge it, decreasing the potential linearly back to the initial level. The potential is recorded as a function of time throughout the cycle, allowing the calculation of specific capacitance, energy density, power density, and evaluation of cycle stability, providing a comprehensive performance profile of the supercapacitor materials [5].

Specific Capacitance Calculation:

The specific capacitance (C) is calculated from the discharge curve using the formula:

$$C_s = \frac{I \cdot \Delta t}{\Delta V \cdot m} \quad (05)$$

where I is the constant current, Δt is the discharge time, ΔV is the voltage change during discharge, and m is the mass of the active material in the electrode [3].

Energy and Power Density:

The energy density (E) and power density (P) of the supercapacitor can be estimated using the specific capacitance values and the operating voltage range:

$$E = \frac{1}{2} C (\Delta V)^2 \quad (06)$$

$$P = \frac{E}{\Delta t} \quad (07)$$

where Δt is the discharge time [3].

1.10.3 Electrochemical Impedance Spectroscopy (EIS):

Electrochemical Impedance Spectroscopy (EIS) is a powerful and versatile technique used to investigate the electrochemical properties and behavior of supercapacitors. It involves applying a small, sinusoidal voltage perturbation to the supercapacitor over a wide range of frequencies and measuring the resulting current response. This method provides detailed information about the resistive, capacitive, and inductive properties of the supercapacitor, helping to understand the various processes occurring within the device. The basic setup includes a three-electrode system for fundamental studies, consisting of a working electrode (the supercapacitor electrode material being tested), a counter electrode (e.g., platinum or graphite), and a reference electrode (e.g.,

Ag/AgCl or SCE). For practical device testing, a two-electrode configuration is used, where the supercapacitor has two symmetric electrodes of the same material. The electrochemical cell is filled with an appropriate electrolyte (e.g., aqueous H_2SO_4 or KOH) to facilitate ion transport, and an electrochemical workstation or potentiostat equipped with EIS capabilities applies the voltage perturbation and measures the current response. During EIS, a small AC voltage (typically 5-10 mV) is applied over a range of frequencies (from 1 MHz to 0.01 Hz), ensuring the system remains in the linear response region. The resulting current response is measured to provide the impedance at each frequency. Impedance data is typically represented in Nyquist plots, which display the imaginary component of impedance (Z'') versus the real component (Z'), and Bode plots, which show the magnitude of impedance (|Z|) and phase angle (θ) versus frequency. These plots help visualize the resistive and capacitive properties and understand the frequency-dependent behavior of the supercapacitor [33].

Analysis of EIS Data:

Resistance Components:

Equivalent Series Resistance (ESR): The high-frequency intercept on the real axis of the Nyquist plot represents the ESR, which includes contributions from the electrolyte resistance, the intrinsic resistance of the electrode material, and the contact resistance between the electrode and the current collector [30].

Charge Transfer Resistance (Rct): The diameter of the semicircle in the Nyquist plot at mid-frequencies represents the charge transfer resistance, which is associated with the redox reactions occurring at the electrode/electrolyte interface [33].

Double-Layer Capacitance (Cdl): At low frequencies, the Nyquist plot typically shows a near-vertical line, indicating ideal capacitive behavior. The slope of this line is related to the double-layer capacitance, which arises from the separation of charge at the electrode/electrolyte interface[33].

Warburg Impedance: At very low frequencies, the Nyquist plot may show a 45-degree line, indicative of the Warburg impedance, which is associated with ion diffusion processes within the porous electrode material [29].

Equivalent Circuit Modeling: An equivalent circuit model can be developed to fit the EIS data, typically consisting of resistors, capacitors, and constant phase elements (CPEs) and Warburg impedance. This model helps in quantitatively analyzing the contributions of different electrochemical processes to the overall impedance [34].

1.11 Chemical structure and morphology:

1.11.1 Scanning Electron Microscopy (SEM):

Scanning Electron Microscopy (SEM) is a powerful technique widely used to analyze the surface morphology and structural details of supercapacitor electrode materials at high resolution. This

method provides critical insights into the physical characteristics of the materials, such as particle size, shape, surface texture, and the distribution of various components, which are essential for understanding and optimizing their electrochemical performance [53,54].

Basic Principles of SEM:

Scanning Electron Microscopy (SEM) uses a focused beam of high-energy electrons generated by an electron gun, which is accelerated towards the sample and scanned across its surface in a raster pattern. When the electron beam interacts with the sample, several signals are produced due to electron-sample interactions, including secondary electrons, backscattered electrons, and characteristic X-rays. These signals provide information about the sample's surface topography and composition. Detectors collect the emitted secondary and backscattered electrons, with secondary electrons primarily used to create detailed images of the surface morphology and backscattered electrons providing information about the composition and topography. The detected signals are then processed to form high-resolution images of the sample's surface [55].

Procedure for SEM Analysis:

Sample preparation for Scanning Electron Microscopy (SEM) involves several key steps. First, the sample surface must be cleaned and free of contaminants to obtain high-quality images. The sample is then mounted on a specimen holder using conductive adhesive to ensure electrical conductivity. Non-conductive samples may be coated with a thin layer of conductive material, such as gold or platinum, to prevent charging under the electron beam. The prepared sample is placed in the SEM chamber, which is then evacuated to create a high-vacuum environment. The operator sets the imaging parameters, including the accelerating voltage (typically 1-30 kV), spot size, and working distance. Lower voltages are used for imaging fine surface details, while higher voltages provide deeper penetration and compositional information. The electron beam is scanned across the sample surface, and the emitted signals are detected and converted into a digital image. The magnification can be adjusted to observe the sample at various scales, from low magnification for overall structure to high magnification for detailed surface features [56].

Analysis of SEM Data for Supercapacitors:

Surface Morphology: SEM images reveal the surface morphology of the electrode materials, showing details such as roughness, porosity, and particle size. These characteristics are critical for understanding the electrode's surface area and active sites available for electrochemical reactions.

Particle Size and Shape: SEM can determine the size and shape of particles or nanostructures in the electrode material. Smaller particle sizes and well-defined shapes often contribute to higher surface areas and improved electrochemical performance.

Porosity and Pore Structure: The porosity and pore structure of the electrode material can be analyzed, which is essential for understanding ion transport and electrolyte accessibility within the electrode.

Composite Materials: For composite electrodes (e.g., GO/PANI/ZnO), SEM can show the distribution and interaction of different components within the composite, revealing how well the materials are integrated.

Defects and Degradation: SEM can identify defects, cracks, and degradation in the electrode material, which are important for assessing the material's durability and stability during cycling.

1.11.2 X-ray Diffraction (XRD):

X-ray Diffraction (XRD) is a powerful analytical technique used to study the crystalline structure of materials, including supercapacitor electrodes. XRD provides detailed information about the phase composition, crystallinity, and structural properties of materials, which are critical for understanding and optimizing their electrochemical performance.

Basic Principles of XRD:

X-ray Generation: XRD uses X-rays generated by an X-ray tube, where high-energy electrons are accelerated and collide with a metal target (typically copper). This collision produces X-rays with a characteristic wavelength.

Interaction with the Sample: When these X-rays are directed at a crystalline sample, they interact with the atomic planes within the material. According to Bragg's Law, constructive interference occurs when the X-ray wavelength, the angle of incidence, and the spacing between atomic planes satisfy the condition: [57]

$$n\lambda = 2dsin(\theta) \quad (09)$$

where n is an integer, λ is the X-ray wavelength, d is the distance between atomic planes, and θ is the angle of incidence.

Diffraction Pattern: Constructive interference of the X-rays results in a diffraction pattern, which is unique to the crystalline structure of the material. This pattern consists of peaks at specific angles corresponding to the different atomic spacing within the sample.

Procedure for XRD Analysis

For XRD analysis, the sample preparation involves different steps depending on the type of sample. For powdered samples, the material is often ground into a fine powder to ensure a uniform and random orientation of the crystallites. For thin-film samples, the material is deposited onto a suitable substrate. The prepared sample is then mounted on a sample holder, which is placed in the XRD instrument. During data collection, the X-ray beam is directed at the sample, and the diffracted X-rays are detected by a detector that moves around the sample to measure the intensity of the diffracted X-rays at various angles. The sample is typically rotated to collect a comprehensive diffraction pattern, ensuring that all possible crystal orientations are measured. In the data analysis phase, the resulting diffraction pattern, consisting of intensity versus 2θ (the angle of diffraction), is analyzed to identify the crystalline phases present in the sample. The positions

and intensities of the peaks in the diffraction pattern are compared to reference patterns in crystallographic databases to identify the phases and determine the crystallinity.

Applications in Supercapacitor Evaluation:

XRD is used to identify the different crystalline phases present in electrode materials, such as GO, PANI, and ZnO, which is crucial for understanding the material's composition and its potential electrochemical performance. It provides insights into the degree of crystallinity and the structural properties of the materials, as high crystallinity often correlates with better electrochemical stability and conductivity. For materials that undergo ion intercalation or are doped with other elements, XRD can detect changes in the lattice parameters, indicating successful intercalation or doping. Additionally, XRD can detect lattice strain and defects within the crystalline structure, which can affect the electrochemical performance and durability of the electrode materials.

1.11.3 Energy Dispersive X-ray Spectroscopy (EDS):

Energy Dispersive X-ray Spectroscopy (EDS) is a powerful analytical technique used to determine the elemental composition of materials, including supercapacitor electrodes. EDS provides detailed information about the presence and distribution of elements within a sample, which is critical for understanding and optimizing their electrochemical performance.

Basic Principles of EDS:

X-ray Generation:

- EDS is typically coupled with Scanning Electron Microscopy (SEM) or Transmission Electron Microscopy (TEM). When the electron beam from the SEM or TEM interacts with the sample, it can dislodge inner-shell electrons from the atoms in the sample.

Characteristic X-rays:

The vacancies left by these dislodged electrons are filled by electrons from higher energy levels. This transition releases energy in the form of characteristic X-rays, which are unique to each element.

X-ray Detection:

An EDS detector captures these characteristic X-rays and generates a spectrum that displays the energy peaks corresponding to different elements present in the sample.

Procedure for EDS Analysis:

For EDS analysis, the sample preparation depends on the type of material being examined. Solid samples are typically mounted on an SEM stub using conductive tape or adhesive, ensuring a clean and smooth surface for analysis. For TEM analysis, thin sections of the sample are prepared using techniques such as ultramicrotomy or focused ion beam (FIB) milling.

Once the sample is prepared and placed in the SEM or TEM, the electron beam is focused on the area of interest. The EDS detector collects the emitted X-rays, and the resulting spectrum is analyzed to determine the elemental composition. Peaks in the spectrum correspond to the characteristic X-rays of different elements, allowing for both qualitative and quantitative analysis.

Applications in Supercapacitor Evaluation:

EDS is used to identify and quantify the elements present in supercapacitor electrode materials, such as GO, PANI, and ZnO. This information is crucial for understanding the composition and verifying the presence of specific elements that contribute to the material's electrochemical performance. EDS can detect dopants, contaminants, and element distribution within the sample, providing insights into the material's uniformity and purity.

By mapping the elemental distribution across the sample surface, EDS can reveal inhomogeneities and the distribution of active materials within the electrode. This is particularly important for optimizing the fabrication process and ensuring consistent performance in supercapacitor applications.

Chapter 2 :

Materials and experimental techniques

2.1 Electrodeposition:

2.1.1 Materials:

For the synthesis and characterization of the PANI/GO/ZnO composite used in supercapacitor applications, high-purity chemicals and precise synthesis methods are essential. The following materials were sourced and prepared to ensure the reliability and effectiveness of the experimental procedures.

Table 2: List of chemicals

Chemical Name	Purchased from	Used for
Aniline (99 %, Analytical grade)	Biochem	PANI synthesis
Sulfuric Acid (18.75 M, Analytical grade)	Biochem	PANI Polimerization
Graphene Oxide	Homemade using Hummers method	Electrode coating
Zinc Sulfate Heptahydrate ($ZnSO_4 \cdot 7H_2O$): Analytical grade	Biochem	Precursor for ZnO synthesis
Acetone	Biochem	Cleaning electrodes surfaces
Ethanol	Biochem	Washing & preparation steps

Potentiostat (PALMSENS 4):

Function: This portable potentiostat/ Galvanostat/ Impedance Analyzer (Figure 11) is crucial for controlling electrochemical experiments. It includes a current generator that delivers either a constant voltage or current to the working electrode, maintaining the desired electrochemical potential through feedback mechanisms.

Measurement System: The device is equipped with a precision measurement system that records the electrochemical response of the electrode in real-time. It measures the potential difference between the working electrode and a reference electrode, as well as the current flowing through the electrochemical circuit. The data collected can be stored for further analysis, allowing for detailed study and optimization of electrochemical properties and reactions.

Figure 11: Potentiostat/ Galvanostat/ Impedance Analyzer

Electrochemical Cell:

The electrochemical cell is made of pyrex glass, with a capacity of 100 ml, ideal for small-scale experiments. This cell is equipped with a five-port lid: the cell accommodates the working electrode (WE), the reference electrode (RE), and the auxiliary or counter electrode (CE). This configuration is typically used in electrochemical studies to ensure a controlled environment and easy access for the electrodes and solutions.

Electrodes:

- The Working Electrode used in this study is made of **304 stainless steel** (1x2 cm,2x3cm) which can be either bare or coated with a synthesized polymer layer. This electrode is the primary focus of the electrochemical reactions and coatings being studied.
- The Counter Electrode is a 0.48 cm^2 platinum plate, which serves to complete the electrical circuit by allowing current to flow through the cell. It is positioned parallel to the working electrode to ensure a uniform electric field and even current distribution across the cell.
- The Reference Electrode: A Saturated Ag/AgCl Electrode filled with KCl, 3 % is used to measure or control the potential at the working electrode. The Ag/AgCl electrode has a known potential of +0.197 V relative to the Standard Hydrogen Electrode (SHE), providing a stable reference point for measurements. It is placed close to the working electrode (about 10 mm) in order to minimize the ohmic drop caused by the electrolyte as shown on the figure 12 below:

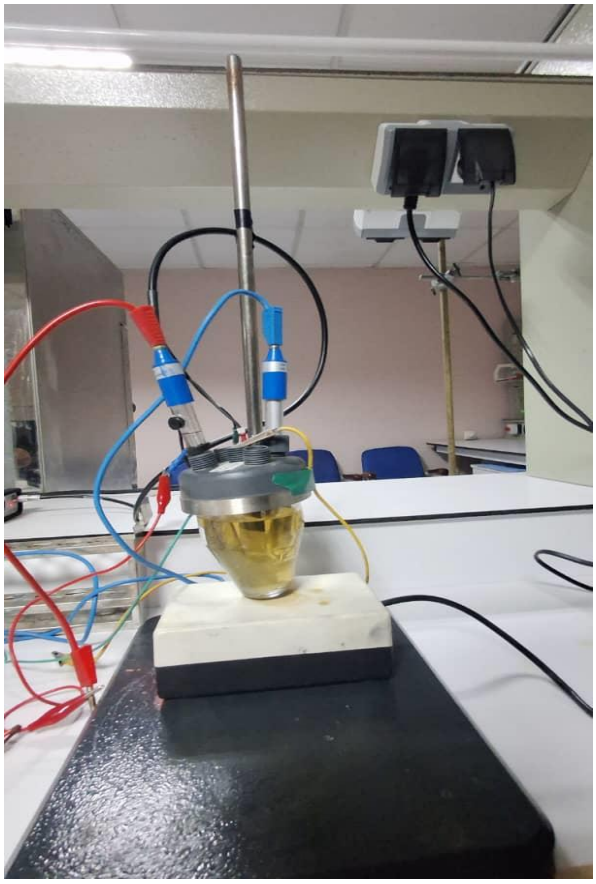

Figure 12: Electrochemical cell setup

Electrolytes:

- The electrolyte used for the electrodeposition of PANI is a combination of two separately prepared solutions: a mixture of 0.5M Aniline and 1M sulfuric acid.
- The electrolyte used for the electrodeposition of GO is a combination of two separately prepared solutions: a dispersion of 0.5 g/Mol Graphene Oxide in 1M sulfuric acid and 0.5M Aniline, which are then mixed together.
- The electrolyte used for the deposition of ZnO is a 0.2M aqueus solution of $ZnSO_4 \cdot 7H_2O$
- The electrolyte used for Electrochemical characterization is a 0.5 M sulfuric acid solution.

2.1.2 Pretreatment:

The stainless steel electrode was meticulously polished using silicon carbide (SiC) papers with progressively finer grain sizes, ranging from coarse to very fine, to achieve an exceptionally smooth and uniform surface (Figure 13). This polishing process ensures that any surface irregularities and contaminants are removed, providing an optimal substrate for electrodeposition. Following the polishing, the electrodes underwent a thorough cleaning process. They were subjected to ultrasonication in acetone to remove any organic residues, followed by ultrasonication in ethanol to further cleanse the surface, and finally rinsed with distilled water to eliminate any

remaining impurities. This multi-step cleaning process guarantees a pristine surface, crucial for consistent and high-quality electrodeposition.

Figure 13:Polisher (materials engineering department)

2.1.3 Electrodeposition of PANI:

To prepare the electrolyte for the electrodeposition of Polyaniline (PANI), a volume of 4.56 mL of Aniline (99%) was dissolved in deionized water to achieve a final volume of 50 ml, leading to a 0.5 M Aniline solution. Next, a 1 M sulfuric acid solution was prepared by carefully adding 2.66 mL of concentrated sulfuric acid to 47.34 mL of deionized water, ensuring to always and carefully add the acid to the water to prevent exothermic reactions. Once both solutions were prepared, equal volumes of the 0.5M aniline solution and the 1M sulfuric acid solution were combined, to obtain 100 mL of the final electrolyte.

For the electrodeposition procedure, the stainless steel (SS) working electrode, the platinum counter electrode, and the saturated Ag/AgCl reference electrode were placed into the Pyrex glass cell, ensuring the reference electrode was positioned close (about 2 mm) to the working electrode. The electrochemical cell was connected to the PalmSens 4 potentiostat. The potentiostat was set up to perform cyclic voltammetry (CV) with a potential range from -0.2 V to 1.2 V at a scan rate of 0.03 V/s, and the CV was run for 31 cycles. During the electrodeposition process, the potential difference between the working electrode and the reference electrode, as well as the current flowing through the electrochemical circuit, were monitored in real-time. The collected data were stored for further analysis to study and optimize the electrochemical properties and reactions Figure 14, 15 and 16). This protocol ensured the preparation of a consistent electrolyte and the

controlled deposition of PANI on the stainless steel substrate.

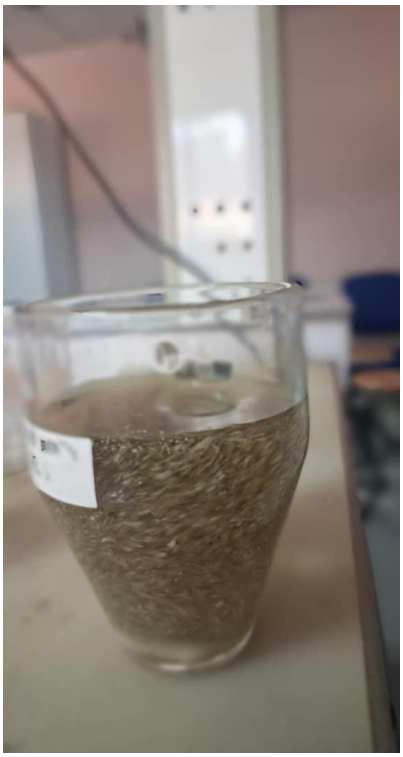

Figure 16:PANI electrolyte before stirring

Figure 15:PANI electrolyte after stirring

Figure 14:PANI electrolyte after electrodeposition

2.1.4 Electrodeposition of PANI/GO:

To prepare the electrolyte for the electrodeposition of the PANI/GO composite, a dispersion of 0.02 g of graphene oxide (GO) in 1M sulfuric acid was first created, resulting in a 0.4 g/L GO solution, using ultrasonication to ensure thorough mixing. Concurrently, a 0.5M aniline solution was prepared as previously reported (section 2.1.3).

For the electrodeposition procedure, the electrochemical cell was connected to the PalmSens 4.9 potentiostat, which was set up to perform cyclic voltammetry (CV) within a potential range from -0.2 V to 1.2 V at a scan rate of 0.01 V/s for 25 cycles. Throughout the electrodeposition process, the potential difference between the working electrode and the reference electrode, as well as the current flowing through the electrochemical circuit, were monitored in real-time. The collected data were stored for subsequent analysis to study and optimize the electrochemical properties and reactions. This protocol ensured the effective incorporation of GO into the PANI matrix, enhancing the properties of the composite electrode on the stainless steel substrate (Figure 17,18) .

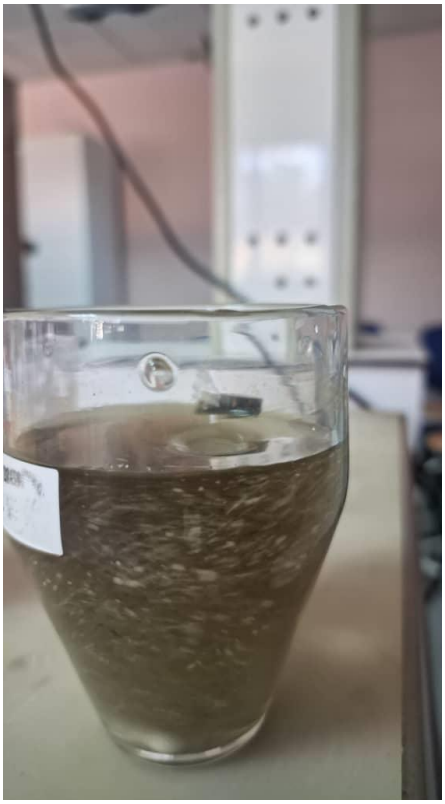

Figure 17:PANI/GO electrolyte before electrodeposition

Figure 18:PANI/GO electrolyte after electrodeposition

2.1.5 Electrodeposition of PANI/ZnO:

To prepare the electrolyte for the ZnO electrodeposition, an amount of 5.75 g of $ZnSO_4 \cdot 7H_2O$ salt was dissolved in 100 mL of a 0.5M sulfuric acid solution using magnetic stirring to get a homogeneous solution. For the PANI/ZnO sample, the electrolyte was prepared by mixing 50 mL of the $ZnSO_4$ solution with 50 mL of the Aniline solution.

For the electrodeposition procedure, the stainless steel (SS) electrode covered with the composites working electrode, platinum counter electrode, and saturated Ag/AgCl reference electrode were placed into a Pyrex glass cell. The electrochemical cell was connected to the PalmSens 4 potentiostat, which was set up to perform cyclic voltammetry (CV) within a potential range from -0.2 V to 1.2 V at a scan rate of 0.03 V/s for 31 cycles, this protocole was also used for the PANI/ZnO sample.

2.1.6 Electrodeposiotion of PANI/GO/ZnO:

For the PANI/GO/ZnO sample, the electrodeposition was performed from (-1 V to 1 V) at a scan rate of 0.01 V/s for 25 cycles. This protocol ensured the effective deposition of ZnO on the PANI and PANI/GO composites, enhancing the properties of the composite electrodes.

Finally, 4 electrodes samples were obtained by the electrodeposition technique: (PANI, PANI/GO, PANI/ZnO,P ANI/GO/ZnO). Later, those 4 samples of electrodes will be used in order to evaluate their electrical performances.

2.2 Electrochemical charachterization:

2.2.1 Cyclic voltammetry (CV):

To perform the cyclic voltammetry (CV) tests on the samples, an electrolyte of 0.5M sulfuric acid was prepared by carefully adding the appropriate amount of concentrated sulfuric acid to deionized water. The stainless steel (SS) working electrode, platinum counter electrode, and saturated Ag/AgCl reference electrode were placed into a Pyrex glass cell. The electrochemical cell was connected to the PalmSens 4.9 potentiostat. Cyclic voltammetry was performed within a potential range from (-0.2 V to 1 V) with varying scan rates of 10, 30, 50, and 100 mV/s. Throughout the CV tests, the potential difference between the working electrode and the reference electrode, as well as the current flowing through the electrochemical circuit, were monitored in real-time. The data was recorded and saved using the PSTrace software (annex) for further analysis. This protocol ensured the thorough characterization of the electrochemical properties of the samples under different scan rates.

2.2.2 Galvanostatic charge-discharge (GCD):

To perform the Galvanostatic Charge-Discharge (GCD) tests on the samples, the same 0.5 M sulfuric acid electrolyte used for the CV tests was utilized. The stainless steel (SS) working electrode, platinum counter electrode, and saturated Ag/AgCl reference electrode were placed into a Pyrex glass cell. The electrochemical cell was connected to the PalmSens 4 potentiostat, which was set up to perform multistep potentiometry using the PSTrace software (annex).

For the GCD tests, the samples were charged to a specific voltage value by applying a positive current of approximately 1 A/g, and then discharged to another voltage value by applying the negative current value. The test parameters were carefully controlled and monitored in real-time. The data collected during the charge-discharge cycles were saved using the PSTrace software (annex) for subsequent analysis.

This protocol ensured the accurate assessment of the charge-discharge behavior and the capacitance of the samples, providing valuable insights into their electrochemical performance. The data collected was then plotted to further investigate the capacitance and other related properties of the samples.

2.2.3 Electrochemical Impedance Spectrospcopy (EIS):

To perform the Electrochemical Impedance Spectroscopy (EIS) test, the same electrolyte used for the CV and GCD tests was used (0.5M sulfuric acid). The stainless steel (SS) working electrode, platinum counter electrode, and saturated Ag/AgCl reference electrode were placed into a Pyrex glass cell. The electrochemical cell was connected to the PalmSens 4 potentiostat, and the test was configured using the PSTrace software.

For the EIS test, the setup was configured to perform a frequency scan over the range of 100000 Hz to 0.01 Hz with an excitation potential of 0.2 V. Throughout the test, the impedance response

of the system was monitored in real-time. The collected data were saved in the form of Nyquist and Bode plots, as well as equivalent circuit fitting results, using the PSTrace software.

This protocol ensured a comprehensive analysis of the impedance characteristics of the samples, providing valuable insights into their electrochemical behavior and properties. The data collected was used for further analysis and interpretation of the equivalent circuit model.

2.3 surface characterization:

2.3.1 Scanning Electron Microscopy (SEM):

Scanning Electron Microscopy (SEM) was utilized to investigate the surface morphology of the synthesized samples. The SEM images were captured using the JEOL JCM-7000 instrument (Figure 19). The experimental conditions for imaging were set as follows:

Magnifications: The samples were examined at two different magnifications: 5000x and 10000x. These magnifications were chosen to provide detailed views of the surface features and overall morphology of the materials.

Acceleration Voltage: An acceleration voltage of 15 kV was applied during imaging. This voltage is optimal for achieving a good balance between resolution and penetration depth, allowing for clear and detailed images of the sample surfaces.

The samples were carefully prepared and mounted on SEM stubs using conductive carbon tape to ensure good conductivity and minimize charging effects.

Overall, the SEM analysis performed under these specific conditions allowed for a comprehensive examination of the sample surfaces, contributing to a better understanding of the material properties and their potential impact on supercapacitor performance.

Figure 19: Scanning Electron Microscopy (Jeol-JCM-7000) (Mining engineering department).

2.3.2 Energy Dispersive X-Ray Spectroscopy (EDS):

Energy Dispersive X-Ray Spectroscopy (EDS) analysis was conducted using the JEOL JCM-7000 instrument (Figure 19) in order to determine the elemental composition and distribution of the synthesized samples. The analysis was performed at an acceleration voltage of 15 kV, consistent with the SEM imaging conditions, to ensure optimal excitation of characteristic X-Rays from the sample elements. After capturing SEM images, EDS was conducted on the same areas to collect emitted X-Rays, generating spectra that display energy peaks corresponding to different elements. Elemental mapping and point analysis were carried out to identify and quantify the elements present and to examine their distribution across the sample surface.

2.3.3 X-Ray diffraction:

The X-Ray Diffraction (XRD) test was conducted at the laboratory of the Centre for Development of Advanced Technologies (CDTA), Figure 20. The difractograms were recorded using the D8Advance XRD instrument (BRUKER axs) at room temperature. This instrument is equipped with a Cu-Kα radiation source with a wavelength of 1.5406 Å. The measurements were taken over 2θ angles ranging from 5° to 80°. This range of angles allows for the examination of a wide variety of crystalline planes, providing detailed information about the composition and crystalline structure of the analyzed samples.

Figure 20: The XRD analysis (CDTA).

Chapter 3 :

Results and interpretations

3.1 Electrodeposition:

The results of the electrodeposition are shown in the table 3 below. These results were obtained after each electrodeposition. The electrodes (Figure 21) were carefully dried and weighted.

Table 3: Composite mass after electrodeposition of each element.

Electrode	Mass before electrodeposition (g)	Mass after electrodeposition (g)	Cycles	Composite mass (g)
PANI	1.498	1.512	31	0.014
PANI/ZnO	1.656	1.674	31	0.018
PANI/GO	1.467	1.489	25	0.022
PANI/GO/ZnO	1.490	1.515	25	0.025

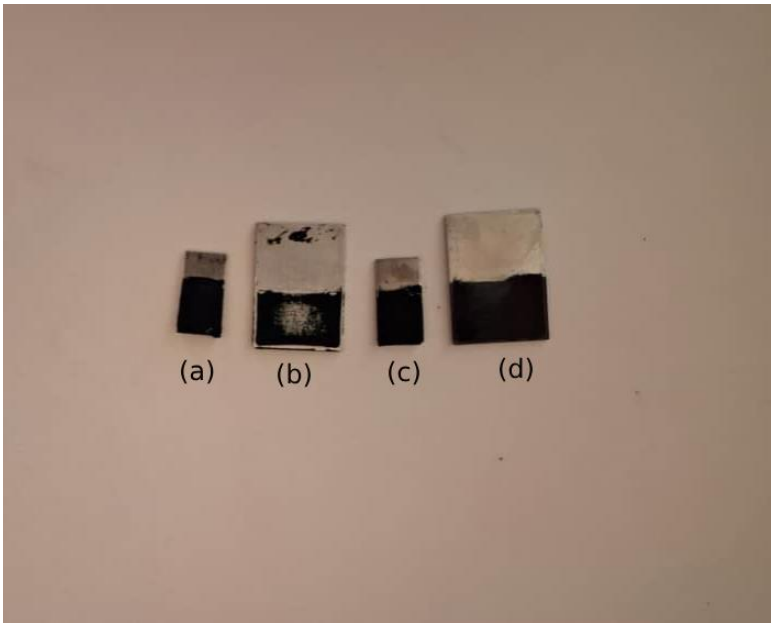

Figure 21: Electrode samples prepared by electrodeposition.(a) PANI/GO/ZnO (b) PANI (c) PANI/GO (d) PANI/ZnO

The results reported on the Table 3 shows that the amount of electrodeposited material increases in proportionally depending on the electrodeposited element. We choose to apply 25 cycles for each electrodeposition in accordance with a previous study in our laboratory (S. OUETTAR & al., 2023) except for PANI which was deposited within 31 cycles. The results show that beyond 25 cycles the electrodeposited material tends to easily separate due to the heavy layer. That is why we only recorded 14 mg of electrodeposited PANI.

Finally, the electrodeposited materials are in perfect accuracy with the results in the bibliography [35] for the electrode surface used (1x2 cm,2x3cm).

Electrodeposition of PANI:

For the electrodeposition of PANI the CV data was plotted on the Figure 22 below:

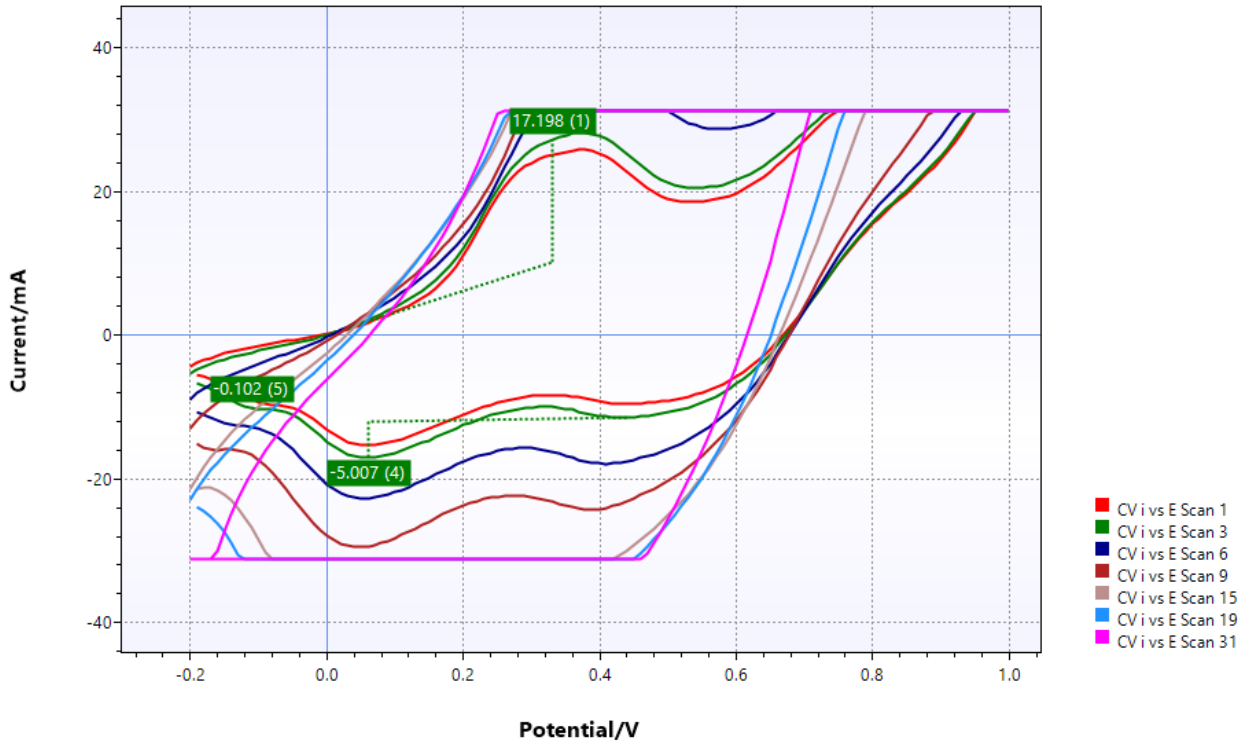

Figure 22: Electrodeposition of PANI- Potential range from -0.2 V to 1.2 V at a scan rate of 0.03 V/s, and the CV was run for 31 cycles.

The provided plot shows the cyclic voltammetry (CV) curves for the electrodeposition of polyaniline (PANI) across multiple scans (Scan 1, Scan 3, Scan 6, Scan 9, Scan 15, Scan 19, and Scan 31). In the initial scans (Scan 1, Scan 3), the CV curves display characteristic redox peaks, indicating the initiation of PANI electrodeposition. The anodic peaks (oxidation) and cathodic peaks (reduction) become more defined as the scan progresses, suggesting the formation of the PANI film on the electrode surface. By Scan 6 and Scan 9, the redox peaks become more pronounced, and the current response increases, indicating the continued growth and increased thickness of the PANI film. The CV curves start to show a more rectangular shape, suggesting improved capacitive behavior due to the increasing surface area of the deposited PANI. In the latest scans (Scan 15, Scan 19, Scan 31), the redox peaks are well-defined, and the current response is significantly higher compared to the initial scans. The CV curves maintain a rectangular shape with prominent redox peaks, indicating the stable and reversible redox processes of the fully formed PANI film.

The anodic peaks observed around 0.2 V to 0.8 V represent the oxidation of aniline monomers to form the polaronic and bipolaronic forms of PANI, this result is in accordance with previous works

(A. KORENT & al., 2020). The shift in peak potential and increase in peak current with successive scans indicate the progressive deposition and growth of the PANI layer. The cathodic peaks, observed in the reverse scan, correspond to the reduction of the oxidized PANI back to its leucoemeraldine state (Figure 23).

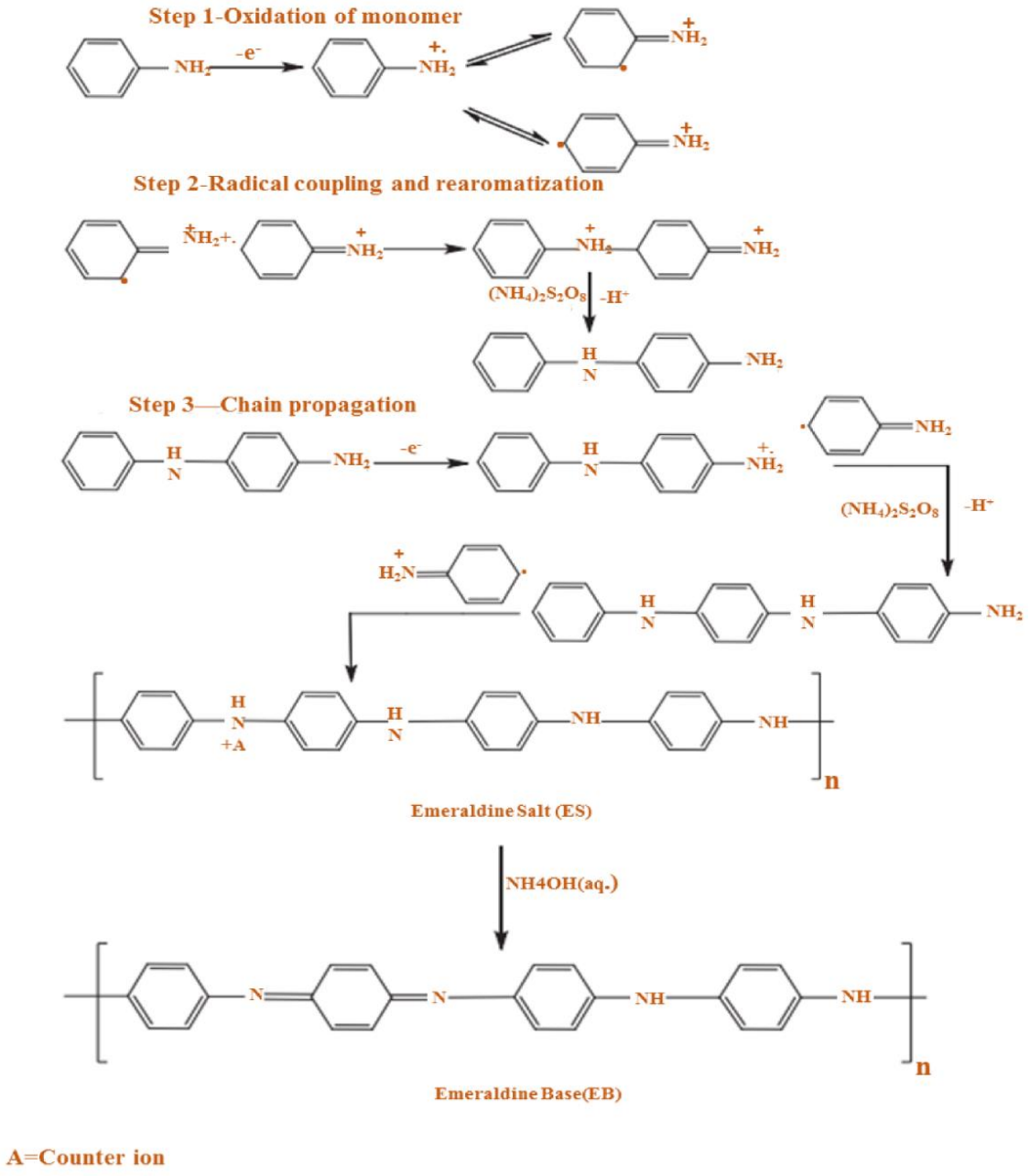

Figure 23:PANI with oxidative polymerization of aniline. Reproduced from Prog. Polym. Sci., Vol 23, Gospodinova, N.; Terlemezyan, L., Conducting polymers prepared by oxidative polymerization: Polyaniline.[36]

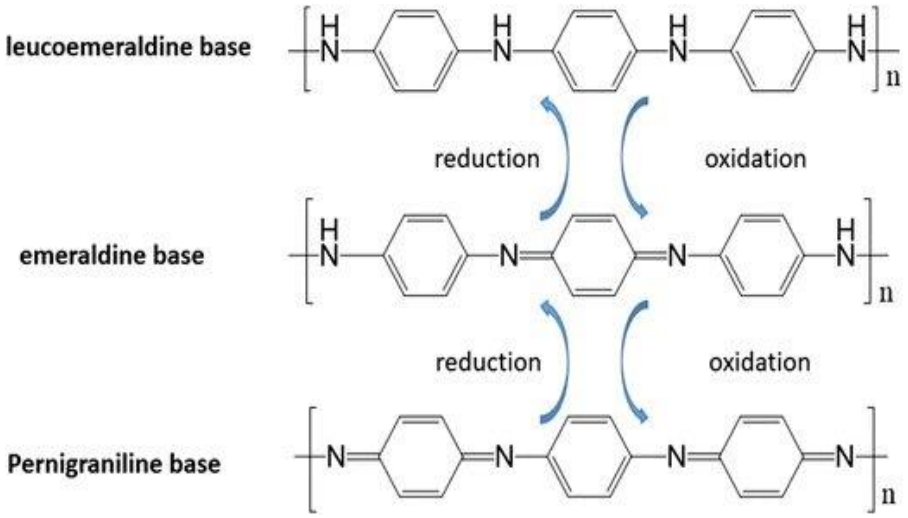

Figure 24:Oxidation-reduction reaction of PANI[37].

Similar to the anodic peaks, the cathodic peaks become more prominent and shifted with successive scans, reflecting the increasing amount of PANI being reduced during the reverse sweep.

In the early stages of electrodeposition, the CV curves exhibit less pronounced capacitive behavior, as the PANI layer is still forming and the surface area is limited. As the PANI layer grows, the CV curves show a more rectangular shape, indicating enhanced capacitive behavior due to the increased surface area and better conductivity of the PANI film [38]. The increasing current response and larger enclosed area in the CV curves reflect the higher charge storage capacity of the thicker PANI layer. Overall, the CV curves for the electrodeposition of PANI display characteristic redox peaks and evolving capacitive behavior across multiple scans. The initial scans show the formation of PANI with defined redox peaks, while the middle and later scans indicate the growth and stabilization of the PANI film with enhanced capacitive properties. The well-defined anodic and cathodic peaks reflect the reversible redox processes of PANI, and the increasing current response suggests the successful electrodeposition and growth of the PANI layer, making it suitable for applications such as supercapacitors and sensors [39].

Electrodeposition of PANI/ GO:

For the electrodeposition of PANI/GO the CV data was plotted on the Figure 25.

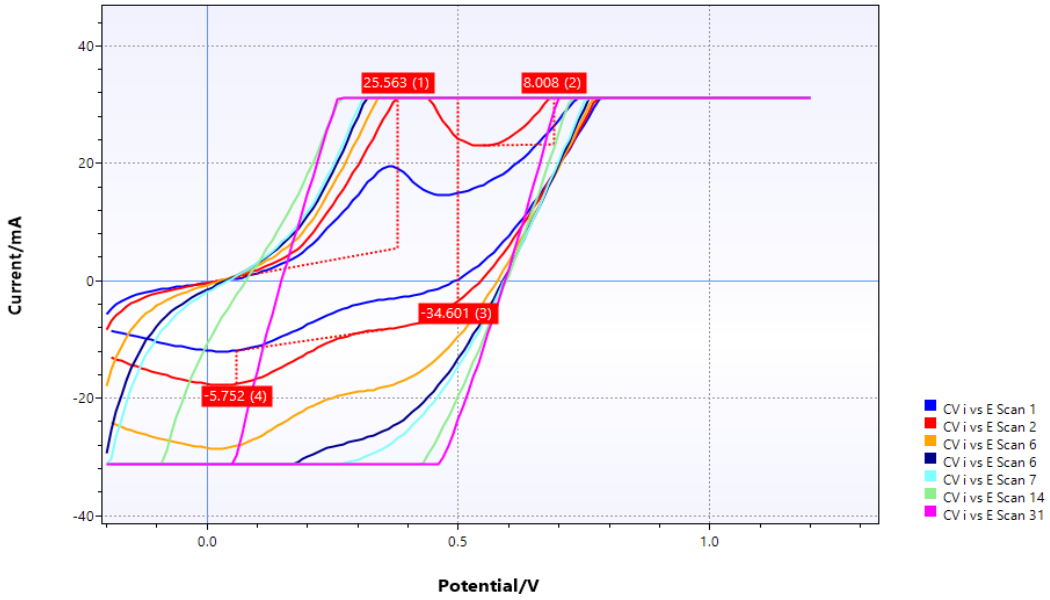

Figure 25 Electrodeposition of PANI/GO- CV performed within a potential range from -0.2 V to 1.2 V at a scan rate of 0.01 V/s for 25 cycles.

The provided cyclic voltammetry (CV) curves for the electrodeposition of polyaniline (PANI) and graphene oxide (GO) on a stainless steel electrode in sulfuric acid (H_2SO_4) electrolyte demonstrate the significant impact of GO incorporation on the electrochemical behavior of the composite. The electrodeposition of PANI primarily occurs during the oxidation process. The oxidation of aniline in sulfuric acid leads to the formation of PANI through the reaction above (Figure 22).

GO, containing oxygen-functional groups such as hydroxyl, epoxy, and carboxyl, interacts with the PANI matrix, facilitating the polymerization of aniline through hydrogen bonding, π-π stacking interactions, and electrostatic interactions. This incorporation of GO results in enhanced current responses, well-defined redox peaks, a more rectangular shape of the CV curves [40].

In the initial scans (Scan 1, Scan 2), the CV curves show the early stages of composite formation with less defined peaks and lower current responses. The oxidation peaks at approximately 0.2-0.4 V correspond to the oxidation of aniline to PANI (Figure 24).

The reduction peaks around 0.4 - 0.6 V correspond to the reduction of PANI back to its leucoemeraldine form.

As the electrodeposition progresses (Scan 6, Scan 9), the redox peaks become more pronounced and the current responses increase, indicating the growth and increased thickness of the PANI/GO composite film. The capacitive behavior becomes evident with a more rectangular shape, reflecting improved charge storage properties [41].

In the later scans (Scan 7, Scan 14, Scan 31), the CV curves exhibit stable and thick PANI/GO films with well-defined redox peaks and a larger area under the curves, indicating higher charge storage capacity. The larger current responses and more defined peaks suggest the enhanced electrochemical activity due to the GO incorporation.

Electrodeposition of ZnO :

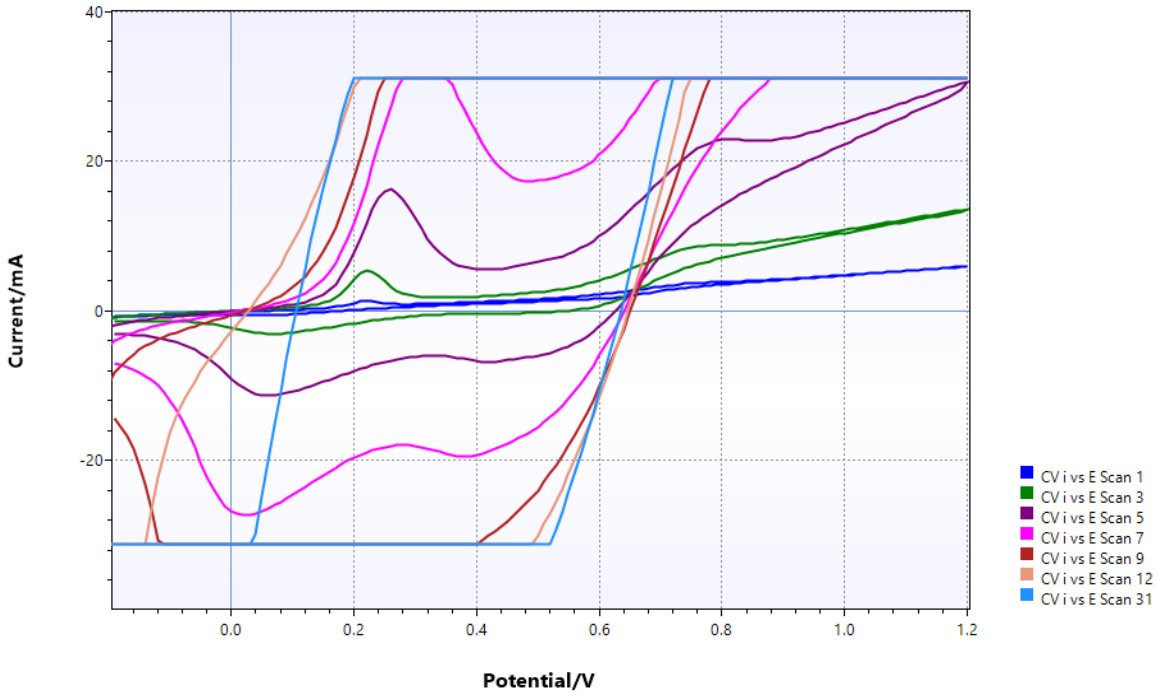

Figure 26:Electrodeposition of PANI/ZnO- potential range from -0.2 V to 1.2 V at a scan rate of 0.03 V/s for 31 cycles.

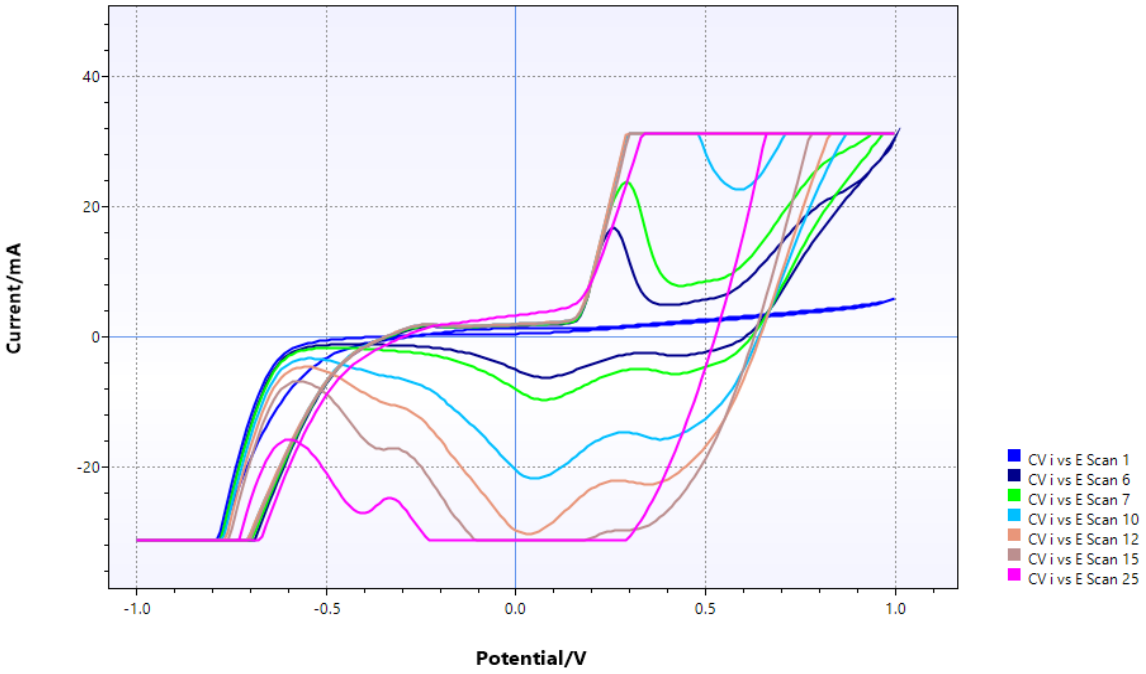

Figure 27:Electrodeposition of PANI/GO/ZnO- performed from -1 V to 1 V at a scan rate of 0.01 V/s for 25 cycles.

The provided cyclic voltammetry (CV) curves for the electrodeposition of polyaniline (PANI), graphene oxide (GO), and zinc ZnO on a stainless steel electrode in a sulfuric acid (H_2SO_4) electrolyte with aniline demonstrate the significant impact of ZnO and GO incorporation on the electrochemical behavior of the composite. The electrodeposition of PANI primarily occurs during the oxidation process. The oxidation of aniline in sulfuric acid leads to the formation of PANI through the following reaction:

$$nC_6H_7N + H_2SO_4 \rightarrow (\mathrm{C_6H_4(NH)^+ - C_6H_4NH_2H^+))n \cdot HSO_4^- + 2H^+ + 2e^-}$$

Zn^{2+}, present in the electrolyte, undergoes deposition during the reduction process, leading to the formation of Zn metal through the following reaction[42]:

$$Zn^{2+} + 2e^- = Zn_{(s)}$$

In the initial scans (Scan 1, Scan 3), the CV curves show the early stages of composite formation with less defined peaks and lower current responses. The oxidation peaks at approximately 0.4-0.8 V correspond to the oxidation of aniline to PANI and the oxidation of zinc to ZnO:

$$Zn_{(s)} + \frac{1}{2}O^2 = ZnO_{(s)}$$

The reduction peaks below 0.4 V correspond to the reduction of PANI back to its leucoemeraldine form and the reduction of Zn^{2+} to Zn [42]:

$$2[C_6H_4(NH)_2]_n + 2H^+ + 2e^- \rightarrow 2nC_6H_7N_2$$

As the electrodeposition progresses (Scan 5, Scan 7) figure 26, the redox peaks become more pronounced and the current responses increase, indicating the growth and increased thickness of the PANI/GO/ZnO composite film. The capacitive behaviour becomes evident with a more rectangular shape, reflecting improved charge storage properties.

In the later scans (Scan 15, Scan 25) figure 27, the CV curves exhibit stable and thick PANI/GO/ZnO films with well-defined redox peaks and a larger area under the curves, indicating higher charge storage capacity [23]. The larger current responses and more defined peaks suggest enhanced electrochemical activity due to the incorporation of ZnO and GO. The combined redox activity of PANI and ZnO provides enhanced charge storage capacity and improved electrochemical performance, making this system suitable for applications in energy storage devices like supercapacitors [43].

Graphene oxide (GO), containing oxygen-functional groups such as hydroxyl, epoxy, and carboxyl, interacts with the PANI matrix, facilitating the polymerization of aniline through hydrogen bonding, π-π stacking interactions, and electrostatic interactions. During the electrodeposition process, GO incorporates into the PANI film, enhancing the electrochemical properties and stability of the composite. This incorporation of GO results in enhanced current responses, well-defined redox peaks, and a more rectangular shape of the CV curves, indicating improved capacitive behavior [44].The presence of GO in the PANI matrix increases the surface area for redox reactions and improves the mechanical stability of the composite film, thus enhancing the overall electrochemical performance of the PANI/GO/Zn composite [42].

The electrodeposition of polyaniline PANI/ GO, PANI/ ZnO, and PANI/ZnO/GO on electrodes results in distinct electrochemical behaviours. PANI deposition primarily occurs during the oxidation of aniline to form the conductive emeraldine salt form, exhibiting well-defined redox peaks and moderate capacitive behaviour [42].The incorporation of GO into PANI enhances current responses and defines redox peaks more sharply due to the interactions between GO's oxygen-functional groups and the PANI matrix, leading to improved capacitive behaviour and electrochemical stability. When ZnO is incorporated into PANI, Zn^{+2} reduce to metallic Zn and they get oxydized to ZnO during the deposition process, increasing overall conductivity and electrochemical activity, resulting in more pronounced redox peaks and higher charge storage capacity[43]. The PANI/ZnO/GO composite demonstrates the highest current responses and the most defined redox peaks, combining the benefits of both GO and Zn. The synergistic effects of GO and ZnO also enhance the mechanical stability and durability of the composite [42].

3.2 Surface and morphology charachterization:

3.2.1 Scanning electron microscopy (SEM):

The SEM images reveal distinct morphological characteristics for each sample, showcasing the effects of different dopants and additives on the structure of polyaniline (PANI).

PANI Sample:

The SEM images of the PANI sample show a nanorod structure with significant agglomeration. This morphology is typical for PANI synthesized by electrochemical methods and indicates a relatively high surface area. The interconnected nanorods form a porous structure, which is beneficial for ion diffusion in electrochemical applications. However, the pure PANI sample exhibits a relatively irregular surface morphology with some degree of agglomeration, which can limit its electrochemical performance due to poorer conductivity and less effective ion transport pathways [14].

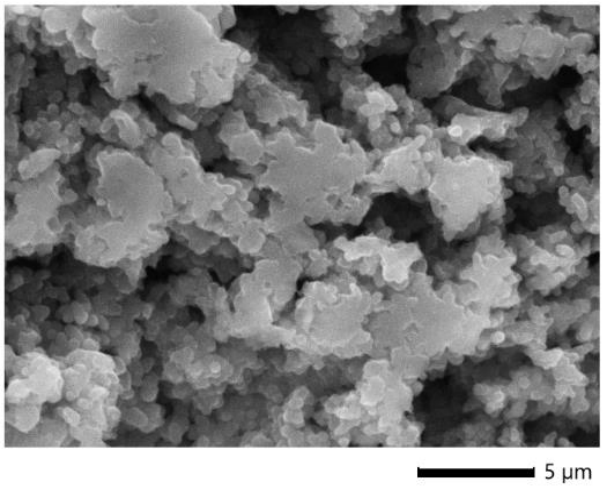

Figure 28: Magnification x5000

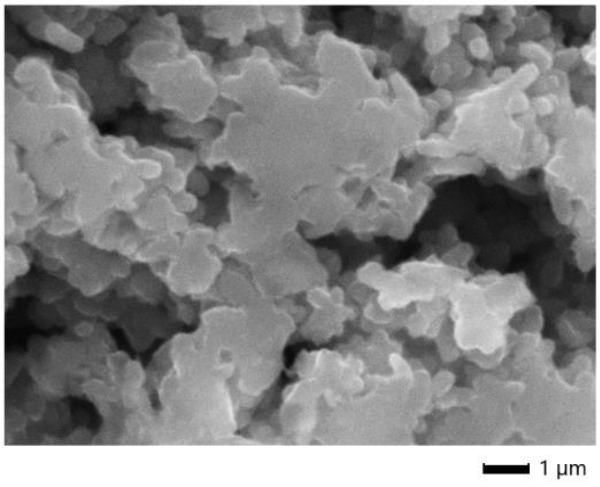

Figure 29: Magnification x10000

PANI/ZnO Sample:

Incorporating Zn ions into the PANI matrix results in noticeable changes in morphology. The ZnO-doped PANI sample displays better-dispersed nanorods compared to the pure PANI. This improved dispersion is attributed to the interaction of Zn ions with the nitrogen sites on the PANI chains, which helps in reducing agglomeration and enhancing the uniformity of the nanorod structure. The Zn doping also introduces more intra- and inter-chain connections, enhancing the overall conductivity of the composite. The SEM images suggest that the ZnO-doped PANI has a more homogeneous surface with fewer agglomerates [21].

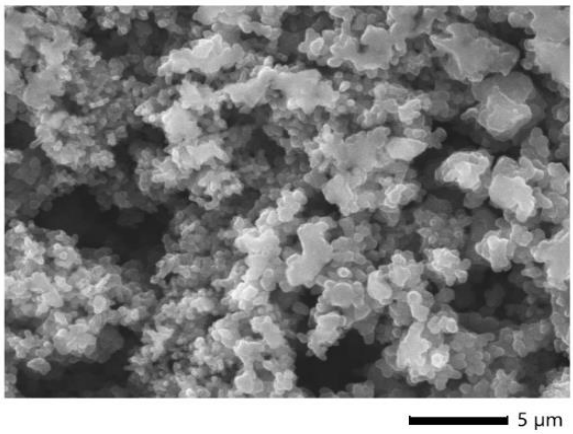

Figure 30: Magnification x5000

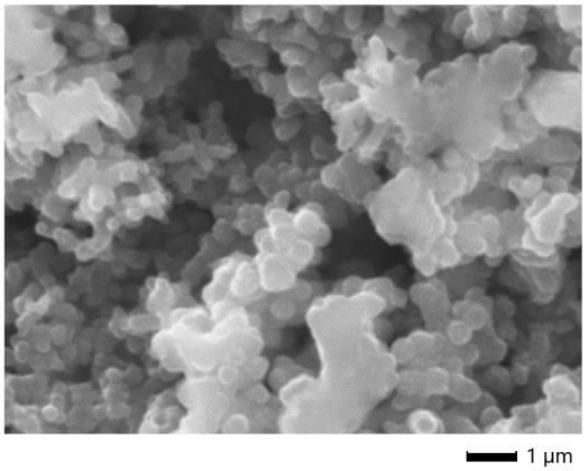

Figure 31: Magnification x10000

PANI/GO:

The addition of graphene oxide (GO) to PANI results in significant morphological changes. The SEM images of the PANI/GO composite show a layered structure with PANI nanorods intercalated between GO sheets. The presence of GO provides a large surface area and facilitates better dispersion of PANI, leading to a more uniform and porous structure. The oxygen-containing functional groups on GO enhance the interaction with PANI, creating strong hydrogen bonds and π-π stacking interactions. This results in improved mechanical stability and higher surface area, which are beneficial for charge storage applications. The PANI/GO composite exhibits a more defined and consistent morphology, which suggests enhanced electrochemical properties due to the synergistic effects of PANI and GO [41].

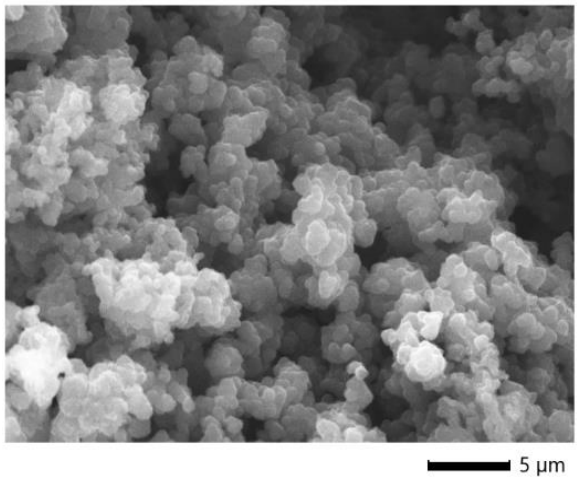

Figure 32: Magnification x5000

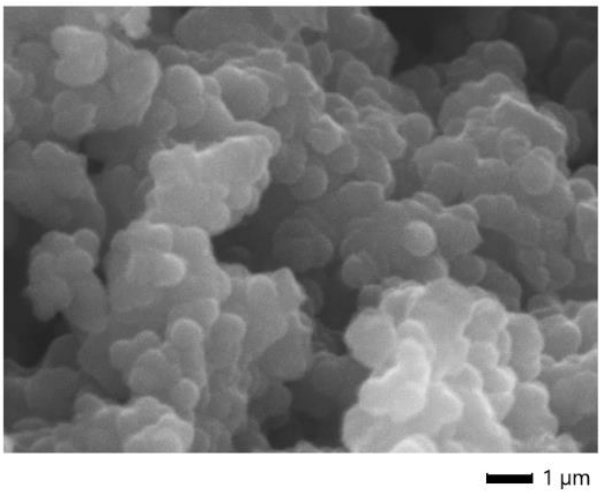

Figure 33:Magnification x10000

PANI/ZnO/GO Sample:

The SEM images of the PANI/ZnO/GO composite display a highly porous and well-dispersed nanorod structure intercalated with GO sheets. This sample combines the benefits of both ZnO doping and GO addition, resulting in superior morphological features. The Zn ions enhance the conductivity of PANI, while the GO sheets provide structural support and prevent agglomeration. The PANI/ZnO/GO composite shows an alternate layered structure with well-defined nanorods and a large number of active sites for electrochemical reactions. This morphology indicates excellent ion diffusion and electron transport properties, which are critical for high-performance supercapacitors. The combined effects of ZnO doping and GO incorporation result in a composite with enhanced specific capacitance, cycling stability, and overall electrochemical performance [42].

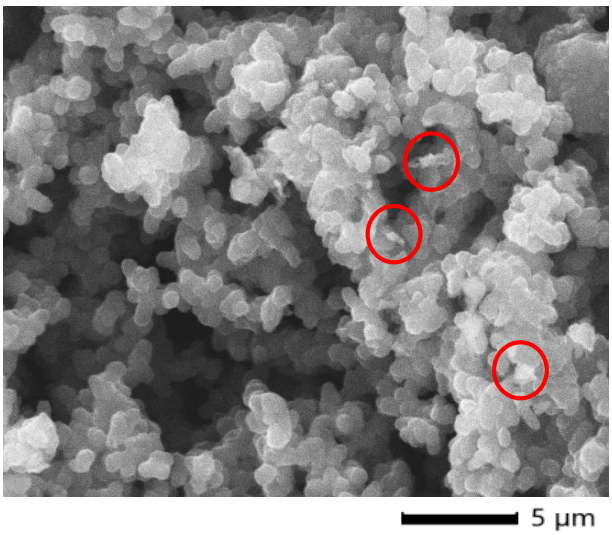

Figure 34: Magnification x5000

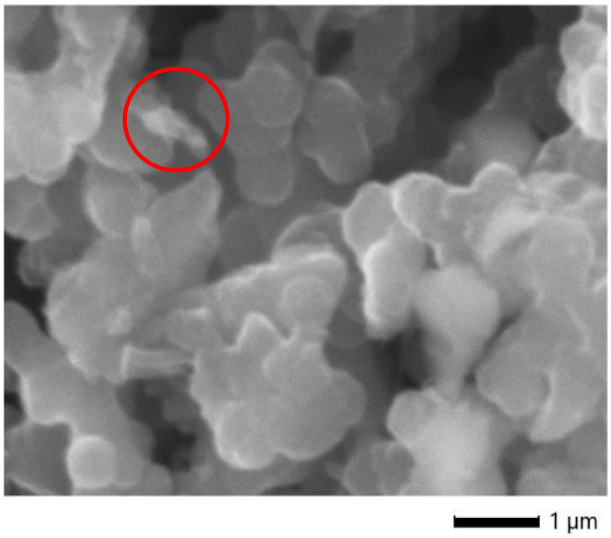

Figure 35:Magnification x10000

Conclusion:

The SEM analysis highlights the significant improvements in morphology and structure when ZnO and GO are incorporated into the PANI matrix. The PANI/ZnO/GO composite exhibits the most favorable characteristics, with a highly porous, well-dispersed, and layered structure, indicating superior electrochemical performance. These enhancements make the PANI/ZnO/GO composite a promising candidate for energy storage applications, , such as supercapacitors, due to its high specific capacitance, improved conductivity, and excellent cycling stability.

3.2.2 Energy Dispersive X-Ray Spectroscopy (EDS):

Interpretation of EDS Analysis for PANI:

The EDS analysis of the pure PANI sample reveals that nitrogen (N) and oxygen (O) are the primary elements present, with nitrogen indicating the presence of the PANI backbone and oxygen suggesting the doping with sulfuric acid (H_2SO_4). The sulfur (S) detected as SO_3 further confirms

the use of sulfuric acid as a dopant. The absence of zinc (Zn) is expected, as this sample does not include ZnO in its composition. The nitrogen content (31.90 ± 1.25% by mass) confirms the PANI structure, while the significant oxygen and sulfur contents indicate successful doping, which is critical for enhancing the conductivity of PANI (Table 4).

Table 4:PANI EDS Elemental Analysis

Element	**Line**	**Mass%**	**Atom%**
N	K	26.57±1.04	33.20±1.30
O	K	48.76±1.25	53.34±1.37
S	K	24.67±0.45	13.46±0.25
Zn	K	nd	nd
Total		100	100

Interpretation of EDS Analysis for PANI/ZnO:

The EDS analysis for the PANI/ZnO sample (Table5) shows the presence of nitrogen (N), oxygen (O), sulfur (S), and zinc (Zn). The nitrogen content (28.86 ± 1.79% by mass) is slightly lower than in pure PANI, while the oxygen content is higher, likely due to the formation of ZnO during the synthesis process. The presence of Zn, although in small amounts (0.90 ± 0.62% by mass), indicates successful incorporation into the PANI matrix. This incorporation is expected to enhance the electrochemical properties by providing additional conductive pathways. The sulfur content remains significant, confirming the use of H2SO4 as a dopant.

Table 5:PANI/ZnO Elemental Analysis

Element	Line	Mass%	Atom%
N	K	28.86±1.79	37.17±2.30
O	K	40.80±1.87	46.01±2.10
S	K	29.44±0.75	16.56±0.42
Zn	K	0.90±0.62	0.25±0.17
Total		100	100

Interpretation of EDS Analysis for PANI/GO:

The PANI/GO sample's EDS analysis shows high nitrogen (N) and oxygen (O) contents, with no detectable zinc (Zn). The nitrogen content (24.37 ± 1.17% by mass) is indicative of the PANI backbone, while the elevated oxygen content reflects the incorporation of graphene oxide (GO), which contains various oxygen-containing functional groups. These functional groups enhance the interaction between PANI and GO, leading to improved stability and electrochemical performance. The sulfur content as SO3 confirms the use of sulfuric acid as a dopant. The absence of Zn is consistent with the sample composition (Table 6).

Table 6: PANI/GO EDS Elemental Analysis

Element	**Line**	**Mass%**	**Atom %**
N	K	24.37±1.17	31.00±1.49
O	K	48.33±1.40	53.83±1.56
S	K	27.30±0.53	15.17±0.30
Zn	K	nd	nd
Total		100	100

Interpretation of EDS Analysis for PANI/ZnO/GO

The EDS analysis for the PANI/Zn/GO sample reveals the presence of nitrogen (N), oxygen (O), sulfur (S), iron (Fe), and zinc (Zn). The nitrogen content (17.71 ± 1.02% by mass) is lower than in the other samples, while the oxygen content is high due to the incorporation of GO. The presence of Zn (2.51 ± 0.65% by mass) indicates successful incorporation into the PANI/GO matrix and indicates that applying a negative dc current is more optimal for electrodeposition of ZnO. The sulfur content remains significant, confirming the use of H2SO4 as a dopant. This complex composition is expected to enhance the composite's electrochemical properties (Table 7).

Table 7: PANI/GO/ZnO EDS Elemental Analysis

Element	**Line**	**Mass%**	**Atom%**
N	K	17.71±1.02	24.29±1.40
O	K	46.56±1.24	55.92±1.50
S	K	29.86±0.54	17.89±0.33
Zn	K	2.51±0.65	0.74±0.19
Total		100	100

Comparison:

Comparing the four samples, the pure PANI sample serves as the baseline with high nitrogen content and significant oxygen and sulfur levels due to H_2SO_4 doping. The PANI/ZnO sample shows successful Zn incorporation, improving conductivity. The PANI/GO sample highlights the benefits of GO, including higher oxygen content and enhanced stability. The PANI/ZnO/GO sample combines the advantages of both ZnO and GO, showing the most complex composition with additional Fe presence, likely enhancing the overall electrochemical performance. The combination of these elements in PANI/ZnO/GO suggests superior conductivity and stability, making it the most promising material for applications in supercapacitors and other energy storage devices.

3.2.3 X-Ray diffraction:

Substrate:

The XRD pattern (Figure 36) for the stainless steel electrode reveals characteristic peaks that correspond to various steel crystal phases. These peaks are indicative of the crystalline structure of the steel, which consists of different phases such as ferrite, austenite, or martensite. The precise location and intensity of these peaks provide insight into the phase composition and structural properties of the steel substrate.

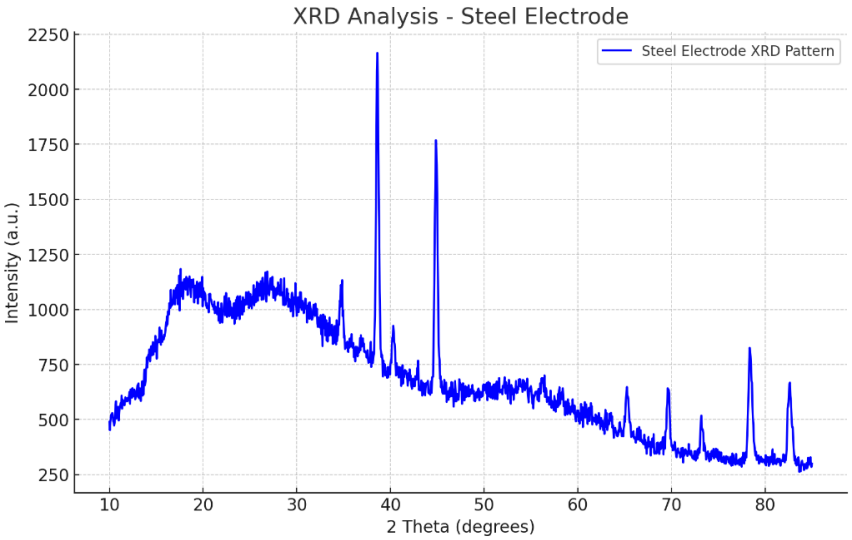

Figure 36: XRD plot for the substrate

PANI:

The XRD pattern for the PANI sample (Figure 37) is characterized by a broad diffuse peak in the range of 19°–30°, which signifies the amorphous nature of polyaniline (PANI). This broad peak is attributed to the disordered arrangement of the polymer chains in PANI. The specific peaks

observed in the plot are due to the underlying steel substrate, indicating that while PANI itself is largely amorphous, the crystalline phases of steel are still detectable in the composite.

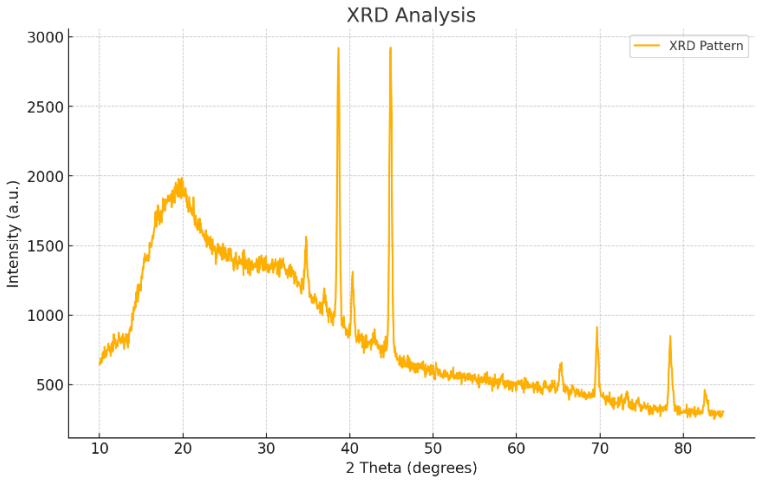

Figure 37: XRD plot for PANI

PANI/GO:

In the XRD pattern for the PANI + GO composite (Figure 38), both polyaniline (PANI) and graphene oxide (GO) contribute to the amorphous nature of the material. This is reflected in the increased intensity observed in the amorphous region. GO, like PANI, exhibits a largely disordered structure, which enhances the overall amorphous character of the composite. The combination of PANI and GO results in a higher degree of amorphousness, which is beneficial for certain applications, such as supercapacitors, where a high surface area and disordered structure can improve performance.

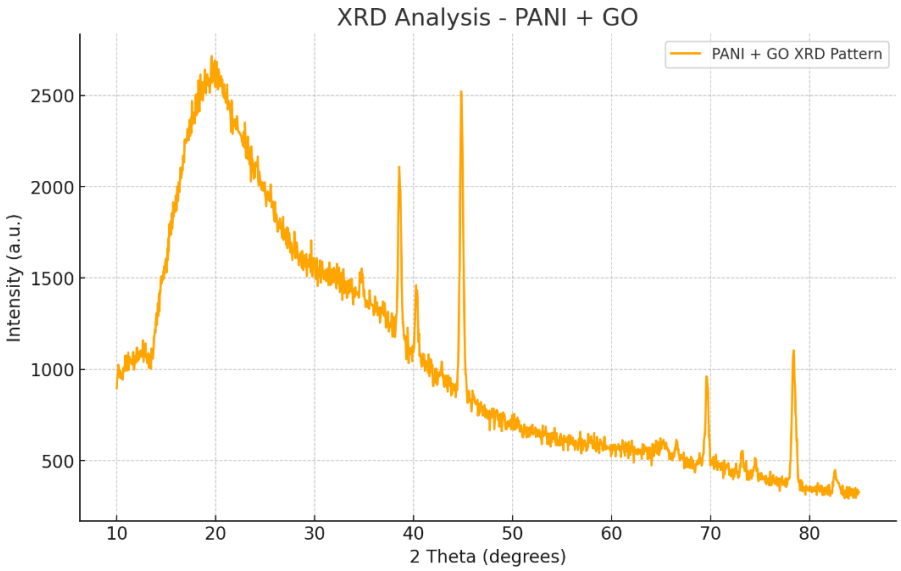

Figure 38: XRD plot for PANI/GO

PANI/GO/ZnO:

The XRD pattern for the PANI + GO + ZnO composite (Figure 39) shows a significant peak at 50.8°, which is attributed to the presence of zinc (Zn). This peak indicates the successful incorporation of Zn into the PANI and GO matrix. The addition of Zn not only introduces new crystalline features but also influences the overall structural properties of the composite. The presence of Zn can enhance the electrical conductivity and mechanical stability of the composite, making it a promising material for applications in energy storage and other advanced technologies.

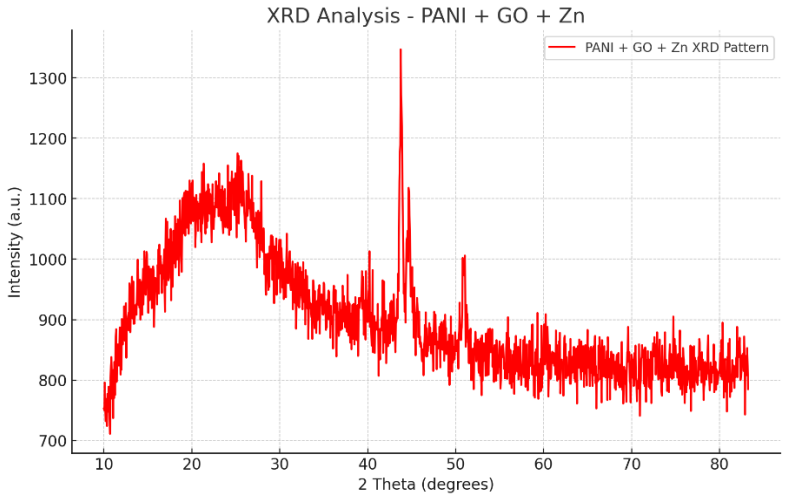

Figure 39: XRD plot for PANI/GO/Zn

3.3 Electrochemical characterization:

3.3.1 Cyclic voltammetry (CV):

- **PANI:**

The cyclic voltammetry (CV) plot for the PANI (polyaniline) electrode at different scan rates (0.01 V/s, 0.03 V/s, 0.05 V/s, and 0.1 V/s) Figure 40, provides insight into the electrochemical behaviour of the material. The charge values calculated from the integrated current for each scan rate are 0.0454 C for 0.10 V/s, 0.1536 C for 0.05 V/s, 0.3740 C for 0.03 V/s, and 3.604 C for 0.01 V/s. The current response increases with increasing scan rates, indicating typical capacitive behaviour, while the shape of the CV curves becomes more rectangular at higher scan rates, reflecting better capacitive properties. The CV curves exhibit clear redox peaks corresponding to the oxidation and reduction processes of PANI, with peak currents increasing with the scan rate, indicating a diffusion-controlled process. However, peak separation increases slightly with scan rate, suggesting some kinetic limitations. Additionally, PANI presents limitations with the AC voltage signal, showing high potential volatility. At higher scan rates, the charge values are relatively lower because the faster sweep rates do not provide sufficient time for the electrochemical processes to fully complete, resulting in lower charge storage. The CV curves at these scan rates are more rectangular, indicating faster charging and discharging cycles but with limited redox activity [37]. At a scan rate of 0.03 V/s, there is a noticeable increase in the charge value, as this intermediate rate allows more time for redox reactions compared to higher scan rates, leading to better charge accumulation. The CV curves show more defined redox peaks, indicating enhanced electrochemical reactions. At the lowest scan rate of 0.01 V/s, the charge value is significantly higher, with the slower sweep rate providing ample time for thorough electrochemical reactions, resulting in maximal charge storage. The CV curves at this scan rate exhibit well-defined redox peaks and larger areas under the curves, reflecting the high charge storage capacity [39].

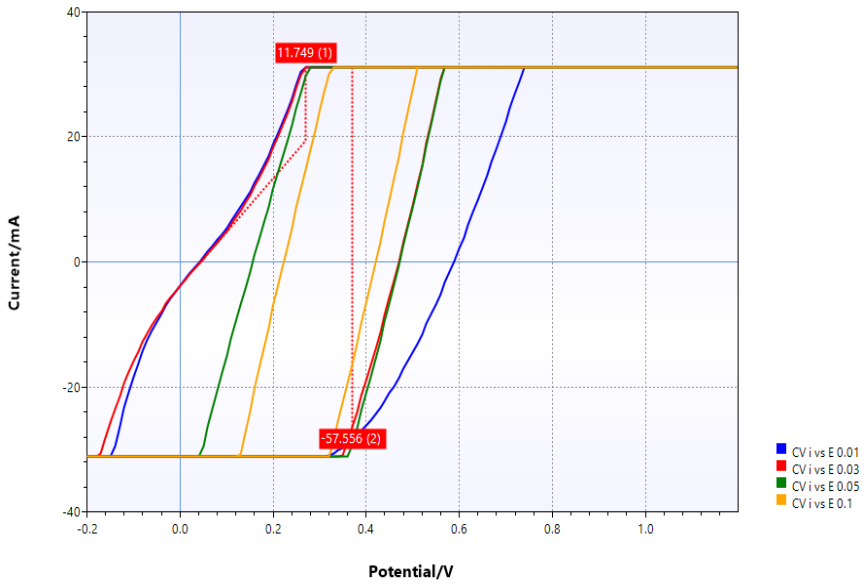

Figure 40: CV plots for PANI at different scanning speeds

- **PANI/GO:**

The provided cyclic voltammetry (CV) curves for the PANI/GO electrode at various scan rates (10 mV/s, 30 mV/s, 50 mV/s, and 100 mV/s) Figure 41 demonstrate the enhanced electrochemical behaviour of the composite material. The calculated charges for different scan rates are as follows: 0.1184 C at 0.1 V/s, 0.3834 C at 0.05 V/s, 0.8663 C at 0.03 V/s, and 3.2540 C at 0.01 V/s. The PANI/GO electrode shows a significant increase in current response with the decrease in scan rate, indicative of the material's enhanced charge storage capacity. The incorporation of graphene oxide (GO) into the polyaniline (PANI) matrix increases the surface area and provides more active sites for electrochemical reactions, leading to higher charge storage. The CV curves exhibit well-defined redox peaks, particularly at lower scan rates, corresponding to the oxidation and reduction processes of PANI. The enhanced redox activity in the presence of GO suggests that GO facilitates faster electron and ion transport, improving the efficiency of redox reactions. The shape of the CV curves becomes more rectangular at lower scan rates, indicating superior capacitive behaviour. This rectangular shape is characteristic of ideal capacitors, where the current is directly proportional to the voltage scan rate [45]. The PANI/GO composite demonstrates improved capacitive performance compared to PANI alone, as shown by the increased charge values. The peak separation remains relatively stable across different scan rates, indicating better kinetic properties. The presence of GO helps in maintaining the structural integrity of the electrode during rapid charge-discharge cycles, reducing the potential volatility commonly observed in pure PANI electrodes. The highest charge per unit voltage at the lowest scan rate (3.254 C at 0.01 V/s) highlights the material's suitability for energy storage applications. The PANI/GO electrode outperforms the PANI electrode in terms of charge storage capacity, stability, and redox activity, making it a promising candidate for supercapacitors and other electrochemical devices. In

summary, the incorporation of GO into the PANI matrix significantly enhances the electrochemical performance of the composite electrode. The PANI/GO electrode exhibits higher current responses, well-defined redox peaks, superior capacitive behaviour, and better stability at various scan rates compared to the PANI electrode. These improvements make the PANI/GO composite a highly effective material for energy storage applications, offering high charge storage capacity and stability [41].

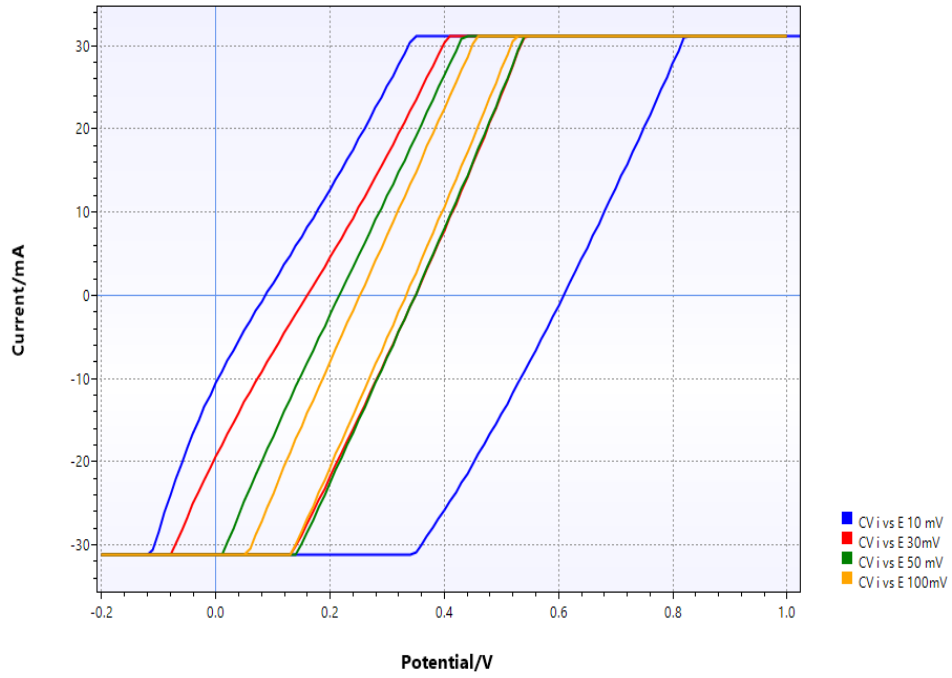

Figure 41: CV plots for PANI/GO at different scanning speeds.

- **PANI/ZnO:**

The provided cyclic voltammetry (CV) curves for the PANI/ZnO electrode at various scan rates (10 mV/s, 30 mV/s, 50 mV/s, and 100 mV/s) Figur 42 demonstrate the electrochemical behaviour of the composite material. The calculated charges for different scan rates are as follows: 0.7067 C at 0.03 V/s, 0.11 C at 0.05 V/s, 0.067 C at 0.1 V/s, and 2.99 C at 0.01 V/s. These values highlight the influence of scan rate on the charge storage capacity of the PANI/Zn composite electrode.

The integration of zinc oxyde (ZnO) into the polyaniline (PANI) matrix demonstrates a noticeable enhancement in charge storage. The current responses increase with decreasing scan rates, which is indicative of higher charge storage efficiency at slower scan rates. The presence of ZnO improves the electrochemical performance by increasing the conductivity and decreasing the overall resistance.

The CV curves reveal well-defined redox peaks, which correspond to the oxidation and reduction processes of PANI and the deposition/dissolution of ZnO. The presence of ZnO enhances the redox

activity, suggesting that ZnO facilitates faster electron and ion transport within the electrode. This is crucial for the efficient operation of supercapacitors, as it ensures rapid charge-discharge cycles.

The PANI/ZnO electrode exhibits more rectangular CV curves at lower scan rates, indicating good capacitive behavior. This shape is a hallmark of materials with high capacitive properties, which are desirable for energy storage applications. The highest charge per unit voltage at the lowest scan rate (2.99 C at 0.01 V/s) emphasizes the material's potential for high-capacity energy storage solutions.

In summary, the incorporation of ZnO into the PANI matrix enhances the electrochemical performance of the composite electrode, particularly in terms of charge storage and stability at various scan rates. The PANI/ZnO electrode shows reasonable current responses, well-defined redox peaks, and good capacitive behaviour. These findings suggest that the PANI/ZnO composite is an effective material for energy storage applications, offering a decent balance between charge storage capacity and stability. However, the overall charge capacity of PANI/ZnO is not as high as that of PANI/GO composites, indicating the superior electrochemical performance of GO in enhancing charge storage [23].

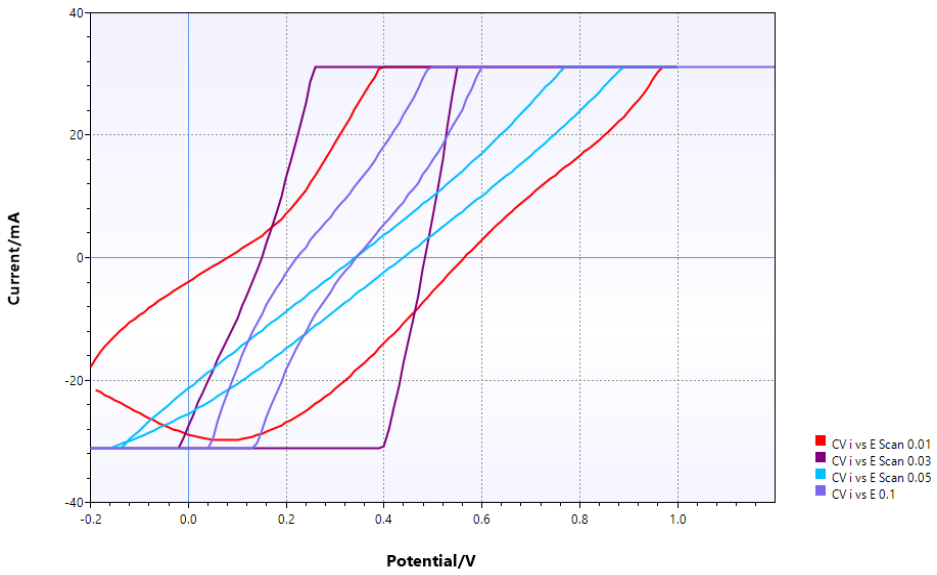

Figure 42: CV plots for PANI/ZnO at different scanning speeds.

- **PANI/GO/ZnO:**

The provided cyclic voltammetry (CV) curves for the PANI/GO/ZnO electrode at various scan rates (10 mV/s, 30 mV/s, 50 mV/s, and 100 mV/s) Figure 43 demonstrate the electrochemical behavior of the composite material. The calculated charges for different scan rates are as follows: 1.0733 C at 0.03 V/s, 0.482 C at 0.05 V/s, 0.1420 C at 0.1 V/s, and 3.2800 C at 0.01 V/s. The incorporation of zinc oxyde (ZnO) and graphene oxide (GO) into the polyaniline (PANI) matrix significantly enhances the charge storage capacity of the composite electrode. The current

responses increase with decreasing scan rates, indicating the composite's high charge storage efficiency.

The PANI/GO/ZnO electrode shows higher charge storage capacity compared to the PANI and PANI/GO electrodes. The incorporation of ZnO and GO improves the electrochemical performance by increasing the surface area and providing more active sites for redox reactions. The well-defined redox peaks in the CV curves correspond to the oxidation and reduction processes of PANI and the deposition/dissolution of ZnO. The enhanced redox activity suggests that the presence of ZnO and GO facilitates faster electron and ion transport, leading to more efficient redox reactions.

The CV curves of the PANI/GO/ZnO electrode exhibit a more rectangular shape at lower scan rates, indicating superior capacitive behavior. The presence of ZnO improves the electronic conductivity, while GO enhances the ion diffusion rate and electron transfer capacity. The combination of these materials results in a composite electrode with improved charge storage and stability. The highest charge per unit voltage at the lowest scan rate (3.28 C at 0.01 V/s) highlights the material's suitability for energy storage applications.

In summary, the incorporation of ZnO and GO into the PANI matrix significantly enhances the electrochemical performance of the composite electrode. The PANI/GO/ZnO electrode exhibits higher current responses, well-defined redox peaks, superior capacitive behaviour, and better stability at various scan rates compared to the PANI and PANI/GO electrodes. These improvements make the PANI/GO/ZnO composite a highly effective material for energy storage applications, offering high charge storage capacity and stability. The presence of ZnO and GO reduces the drop in charge in the case of relatively high potential volatility commonly observed in pure PANI electrodes, making the composite more suitable for practical applications in supercapacitors and other electrochemical devices [23,42].

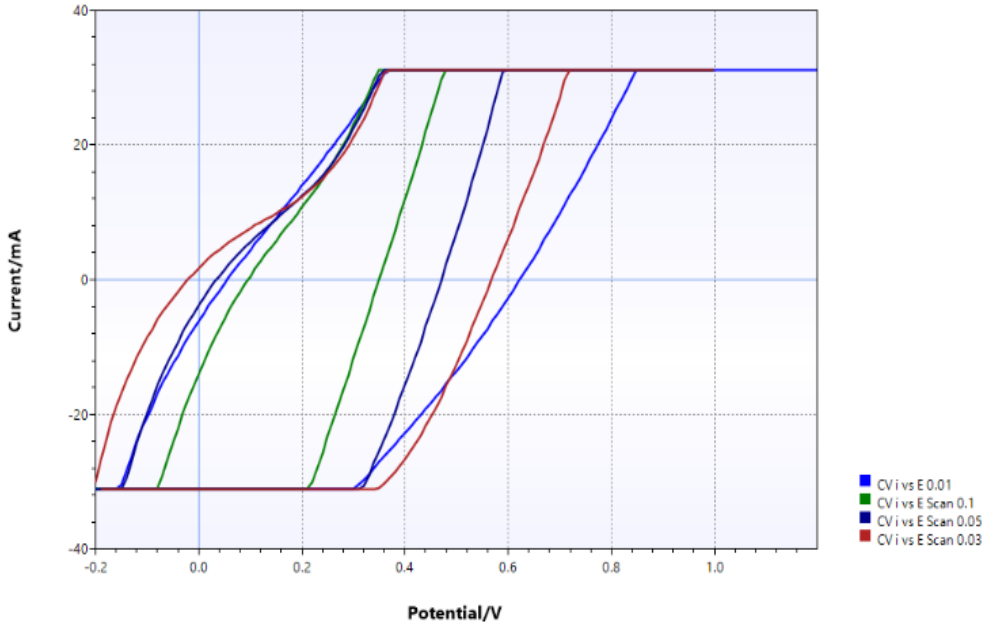

Figure 43: CV plots for PANI/GO/ZnO at different scanning speeds.

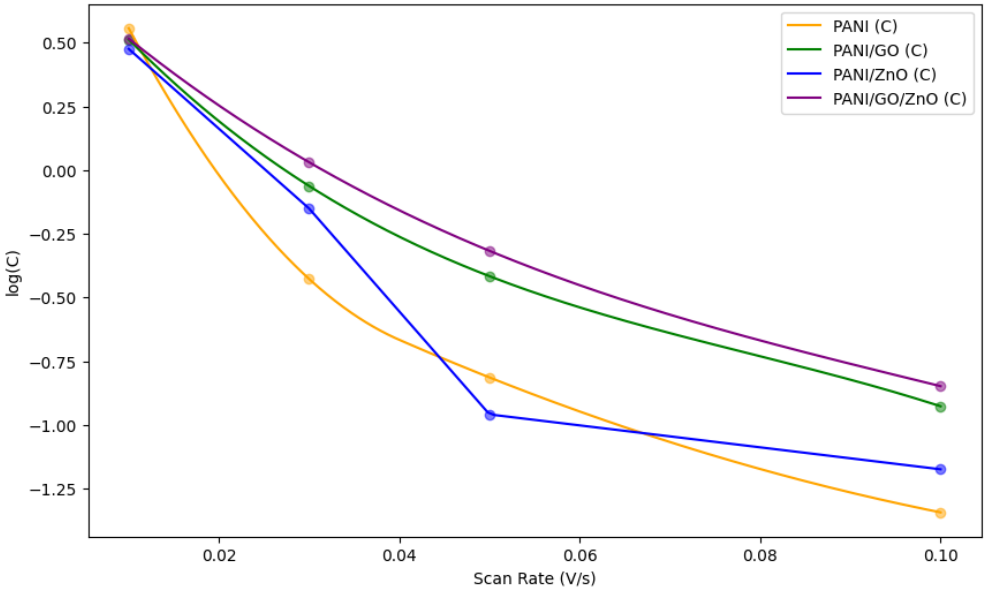

Figure 44 :Plot of Charge vs scan rate on logarithmic scale

Comparison:

The comparison of PANI, PANI/GO, PANI/ZnO, and PANI/GO/ZnO electrodes, based on their cyclic voltammetry (CV) analysis, reveals distinct differences in their electrochemical behaviours and performance in energy storage applications. The logarithmic plot of charge (log(C)) *vs* scan rate (V/s), the charge was calculated using equations (3) and (4) provides insights into the efficiency and stability of these materials under varying conditions. The PANI electrode shows typical capacitive behaviour with high charge storage efficiency at lower scan rates, but its performance significantly drops at higher scan rates, indicating limitations in charge transfer kinetics and potential volatility under AC voltage signals. The PANI/GO electrode demonstrates enhanced performance compared to the PANI electrode. The incorporation of graphene oxide (GO) increases the surface area and provides more active sites for redox reactions, leading to improved charge storage capacity, stability, and reduced potential volatility. The PANI/ZnO electrode exhibits increased conductivity and decreased overall resistance due to the presence of zinc oxide (ZnO) (Figure 44). While it shows better performance than the PANI electrode, its charge capacity is less than that of the PANI/GO electrode, suggesting that ZnO enhances conductivity but does not contribute as significantly to charge storage. The PANI/GO/ZnO electrode outperforms all other samples, exhibiting the highest charge storage capacity, improved stability, and reduced charge drop at higher scan rates. The combined effects of ZnO and GO enhance both the conductivity and the number of active sites, making the PANI/GO/ZnO composite the most promising material for high-capacity energy storage applications. Overall, the PANI/GO/ZnO composite shows the best electrochemical performance among the studied materials, highlighting its potential for use in advanced energy storage systems.

3.3.2 Galvanostatic charge-discharge (GCD):

Analysis of the Charge-Discharge Plot for PANI Electrode:

The charge-discharge data for the PANI electrode indicates a charge time of 111 seconds and a discharge time of 89 seconds, with a voltage change of 0.7 V. The charge capacity is 4.76 F, while the discharge capacity is 3.81 F. This data reveals that the PANI electrode exhibits good capacitive behaviour. The difference in charge and discharge times suggests some energy losses during the process. The efficiency, calculated by comparing the charge and discharge capacities, is approximately 80 %, indicating that 80 % of the stored charge is recoverable during discharge, with 20 % lost. The charge loss can be attributed to the internal resistance of the PANI material and the sulfuric acid (H_2SO_4) electrolyte used in the system. Internal resistance leads to resistive losses, while the sulfuric acid electrolyte may contribute to additional inefficiencies during the electrochemical reactions [14]. The discharge curves of the PANI composites can be divided into two stages: the potential drop range of 0.7–0.34 V is associated with pure electric double-layer capacitance with a relatively short discharge duration, while the range from 0.34–0 V involves both faradic capacitance and pure electric double-layer capacitance, resulting in a relatively long discharge time. Additionally, the plot shows a linear increase and decrease in potential during the charge and discharge cycles, indicative of good capacitive characteristics, suggesting that the

PANI electrode is able to store and release charge effectively. The charge and discharge cycles (Figure 45) are symmetrical, indicating high coulombic efficiency, meaning most of the charge stored during the charging phase is released during the discharge phase, indicating minimal energy losses. Overall, the charge-discharge plot data demonstrates that the PANI electrode has reasonable charge-discharge efficiency, although some charge losses are due to internal resistance and the sulfuric acid electrolyte [1].

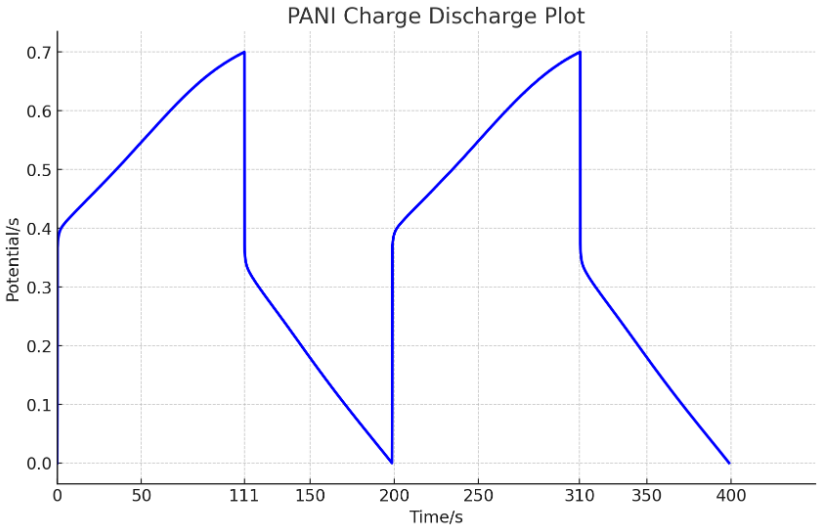

Figure 45 :PANI charge discharge

Analysis of the Charge-Discharge Plot for PANI/GO Electrode:

The charge-discharge data for the PANI/GO electrode indicates that the charge time is 177.7 seconds and the discharge time is 153.1 seconds, with a voltage change of 0.7 V. The charge capacity is recorded at 7.61 F, while the discharge capacity is 6.56 F. This data reveals that the PANI/GO electrode exhibits strong capacitive behaviour, with a notable improvement in charge and discharge capacities compared to pure PANI. The efficiency of the PANI/GO electrode, calculated by comparing the charge and discharge capacities, is approximately 86 %, indicating that 86 % of the stored charge is recoverable during discharge, with 14 % lost. The discharge curve of the PANI/GO electrode can be divided into two stages: the potential drop range of 0.7–0.6 V is associated with pure electric double-layer capacitance with a relatively short discharge duration, while the range from 0.6–0 V involves both faradic capacitance and pure electric double-layer capacitance, resulting in a relatively long discharge time. The plot shows a linear increase and decrease in potential during the charge and discharge cycles, indicative of good capacitive characteristics, suggesting that the PANI/GO electrode is able to store and release charge

effectively. The charge and discharge cycles are symmetrical, indicating high coulombic efficiency, meaning most of the charge stored during the charging phase is released during the discharge phase, indicating minimal energy losses (Figure 46). Overall, the charge-discharge plot data reveals that the PANI/GO electrode demonstrates enhanced charge-discharge efficiency and capacities, although some charge losses are due to internal resistance and the sulfuric acid electrolyte [41].

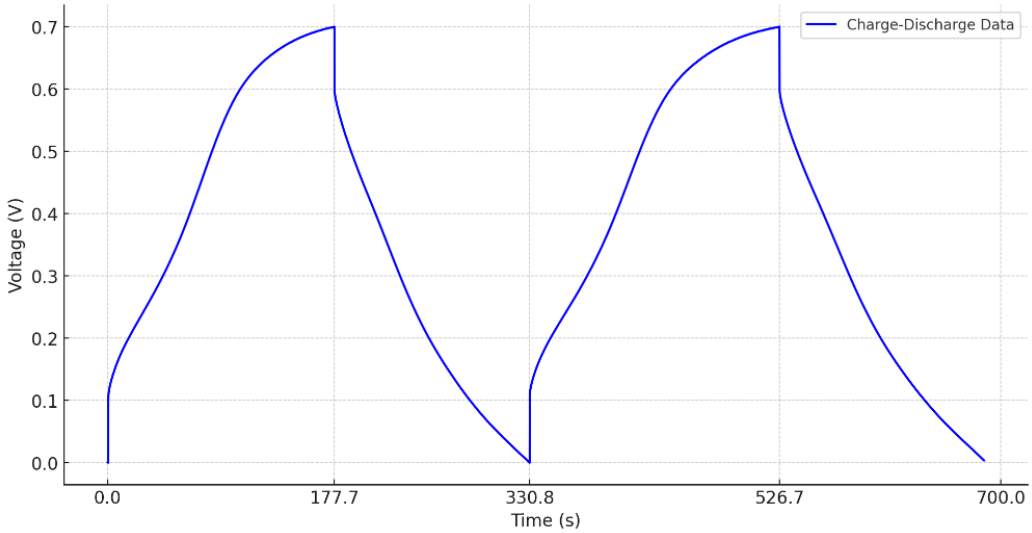

Figure 46:PANI/GO charge discharge plot.

Analysis of the Charge-Discharge Plot for PANI/ZnO Electrode:

The charge-discharge data for the PANI/ZnO electrode shows a charge time of 118.8 seconds and a discharge time of 100 seconds, with a voltage change of 0.7 V. The charge capacity is 5.09 F, while the discharge capacity is 4.29 F. This indicates that the PANI/ZnO electrode has good capacitive behaviour, though slightly lower than the PANI/GO composite. The efficiency of the PANI/ZnO electrode, calculated by comparing the charge and discharge capacities, is approximately 84 %, meaning that 84 % of the stored charge is recoverable during discharge, with 16 % lost. The discharge curve for the PANI/ZnO electrode can be divided into two stages: the potential drop from 0.6 to 0.38 V corresponds to pure electric double-layer capacitance with a relatively short discharge duration, while the range from 0.38 to 0 V involves both faradic capacitance and pure electric double-layer capacitance, resulting in a relatively long discharge time. The plot (Figure 47) shows a linear increase and decrease in potential during the charge and discharge cycles, indicative of good capacitive characteristics, suggesting that the PANI/ZnO electrode is able to store and release charge effectively. The charge and discharge cycles are symmetrical, indicating high coulombic efficiency, meaning most of the charge stored during the charging phase is released during the discharge phase, indicating minimal energy losses. The loss

of charge during discharge is primarily due to the internal resistance of the composite material and the sulfuric acid (H_2SO_4) electrolyte used. Overall, the data from the charge-discharge plot demonstrates that the PANI/ZnO electrode has good charge-discharge efficiency and capacities, although some charge losses are attributed to internal resistance and the sulfuric acid electrolyte.

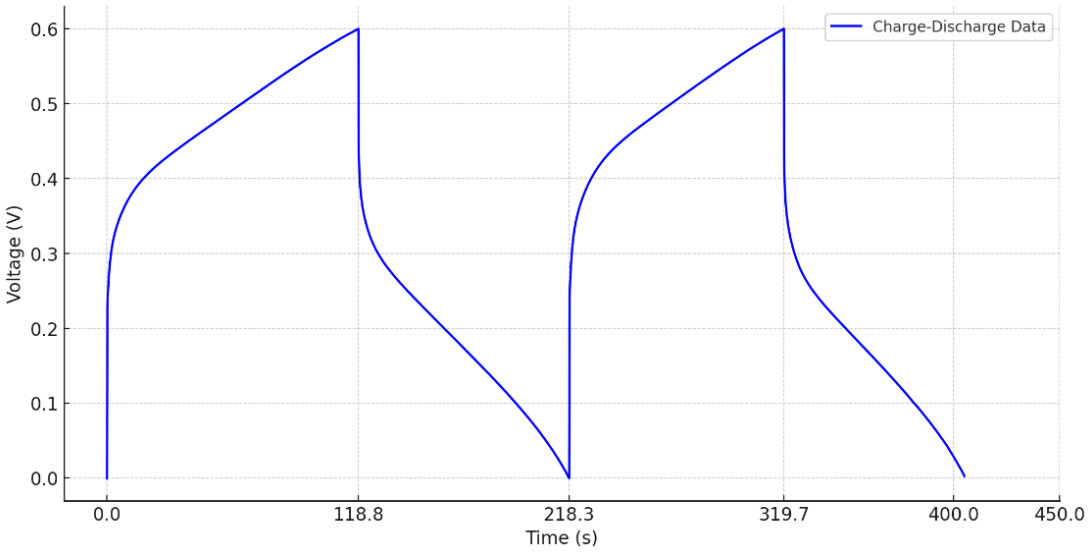

Figure 47 :PANI/ZnO charge discharge plot.

Analysis of the Charge-Discharge Plot for PANI/GO/ZnO Electrode

The charge-discharge data for the PANI/GO/ZnO electrode shows a charge time of 150.9 seconds and a discharge time of 209.8 seconds, with a voltage change of 0.7 V. The charge capacity is 6.47 F, while the discharge capacity is 8.99 F. This indicates that the PANI/GO/ZnO electrode has excellent capacitive behaviour, with significant improvement in both charge and discharge capacities compared to other composites (Figure 48). The efficiency of the PANI/GO/ZnO electrode, calculated by comparing the charge and discharge capacities, is approximately 139 %, meaning that the electrode can discharge more capacity than it initially charged, which is an indicator of an effective energy storage system. The discharge curve for the PANI/GO/ZnO electrode can be divided into two stages: the potential drop from 0.7 to 0.58 V corresponds to pure electric double-layer capacitance with a relatively short discharge duration, while the range from 0.58 to 0 V involves both faradic capacitance and pure electric double-layer capacitance, resulting in a relatively long discharge time. The discharge time being longer than the charging time is due to the incorporation of ZnO and GO, which lowers internal resistance and enhances the overall efficiency of the electrode. The plot shows a linear increase and decrease in potential during the charge and discharge cycles, indicative of good capacitive characteristics, suggesting that the PANI/GO/ZnO electrode is able to store and release charge effectively. The charge and discharge cycles are symmetrical, indicating high coulombic efficiency, meaning most of the charge stored during the charging phase is released during the discharge phase, indicating minimal energy losses. Overall, the data from the charge-discharge plot demonstrates that the PANI/GO/ZnO electrode

has superior charge-discharge efficiency and capacities, attributed to the combined effects of ZnO and GO and the reduced internal resistance [16,23,41].

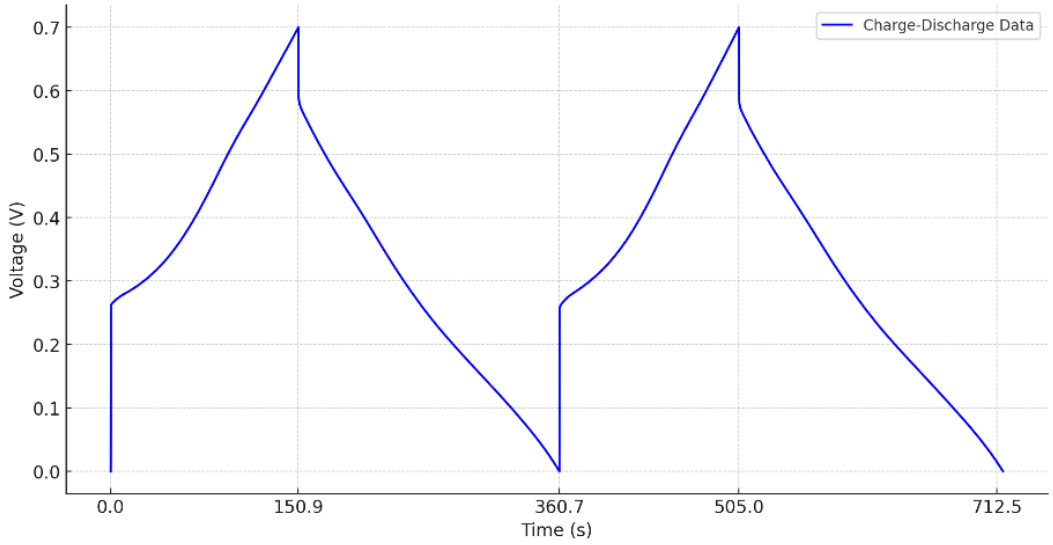

Figure 48 :PANI/GO/ZnO charge discharge

Table 8: Electrode Performance Data for PANI, PANI/GO, PANI/ZnO, and PANI/GO/ZnO

Metric	**PANI**	**PANI/GO**	**PANI/ZnO**	**PANI/GO/ZnO**
Charge Time (s)	111	177.700	118.800	150.900
Discharge Time (s)	89	153.100	100	209.800
Voltage Change (V)	0.700	0.700	0.600	0.700
Charge Capacity (F)	4.760	7.610	5.940	6.470
Discharge Capacity (F)	3.810	6.560	5.000	8.990
Efficiency (%)	80	86	84	139
Mass (g)	0.014	0.022	0.018	0.025
Charging Specific Capacity (F/g)	317.330	345.910	330	258.800
Discharge Specific Capacity (F/g)	254	298.180	277.770	359.600
Energy Density (Wh/kg)	8.550	9.270	7.520	9.800

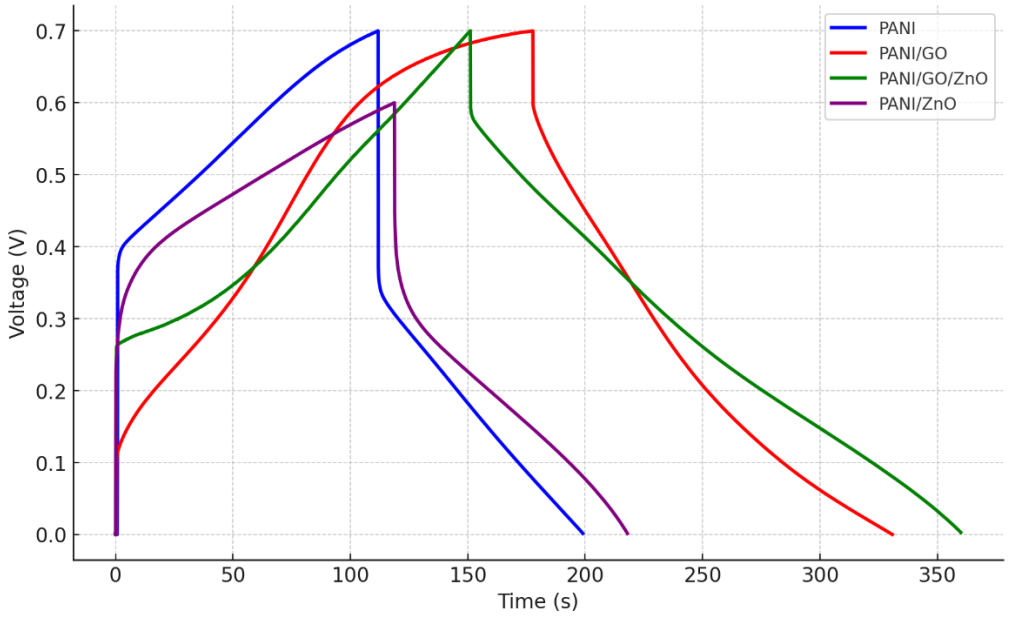

Figure 49 :Comparaison of 1 GCD cycle.

The comparison of electrode performance for PANI, PANI/GO, PANI/ZnO, and PANI/GO/ZnO reveals significant differences in various metrics. The charge and discharge times for PANI are 111 seconds and 89 seconds, respectively, while PANI/GO exhibits the longest charge time at 177.7 seconds and a discharge time of 153.1 seconds. PANI/ZnO shows moderate charge and discharge times at 118.8 and 100 seconds, respectively, whereas PANI/GO/ZnO has a charge time of 150.9 seconds and the longest discharge time at 209.8 seconds. All electrodes maintain a uniform voltage change of 0.7 V. In terms of capacities (Figure 49), Table 8, PANI has a charge capacity of 4.76 F and a discharge capacity of 3.81 F, whereas PANI/GO has the highest charge capacity at 7.61 F and a discharge capacity of 6.56 F. PANI/Zn's charge and discharge capacities are 5.94 F and 4.29 F, respectively, while PANI/GO/ZnO exhibits a charge capacity of 6.47 F and the highest discharge capacity at 8.99 F. Efficiency varies, with PANI at 80%, PANI/GO at 86 %, PANI/ZnO at 84 %, and PANI/GO/ZnO demonstrating the highest efficiency at 139 %. In terms of mass, PANI weighs 0.014 g, PANI/GO 0.022 g, PANI/ZnO 0.018 g, and PANI/GO/ZnO 0.025 g. For specific capacities, PANI/GO has the highest charging specific capacity at 345.91 F/g and PANI/GO/ZnO the highest discharge specific capacity at 359.60 F/g. Energy density is highest for PANI/GO/ZnO at 9.80 Wh/kg. In conclusion, the PANI/GO/ZnO electrode exhibits superior overall performance, with the highest discharge capacity, energy density, and efficiency, making it a strong candidate for applications requiring efficient charge storage and transfer. The PANI/GO electrode also shows excellent performance with the highest charging specific capacity. PANI/ZnO provides balanced performance with good charge transfer efficiency and ion diffusion.

3.3.3 Electrochemical impedance spectrospcopy (EIS):

✓ **PANI:**

The EIS data for the PANI electrode, modeled using an equivalent circuit, includes components such as solution resistance (R1 = 5.803 Ω), charge transfer resistance (R2 = 8.923 Ω), double layer capacitance (C1 = 355.9 µF), and Warburg impedance (W1 = 1 Ω) (Figure 51). The Nyquist plot (Figure 50) shows the real part of the impedance (Z') on the x-axis and the negative imaginary part of the impedance (-Z'') on the y-axis, with the blue line representing measured data and the red line representing fitted data. In the high-frequency region, the plot indicates the dominance of the solution resistance (R1). The mid-frequency range shows a semicircle corresponding to the charge transfer resistance (R2) and double layer capacitance (C1). In the low-frequency region, a linear increase suggests the presence of Warburg impedance (W1), indicating diffusion-controlled processes. The fit between the measured and modeled data is reasonably good, suggesting the appropriateness of the equivalent circuit model. The significant double layer capacitance (C1) indicates a large surface area and good capacitive behavior, while the higher charge transfers resistance (R2) suggests a higher resistance to charge transfer processes. The Warburg impedance (W1) indicates efficient ion diffusion. Overall, the PANI electrode shows promising electrochemical properties for applications requiring efficient charge storage and transfer, although the higher charge transfer resistance suggests that further optimization may be needed to enhance performance [39,46].

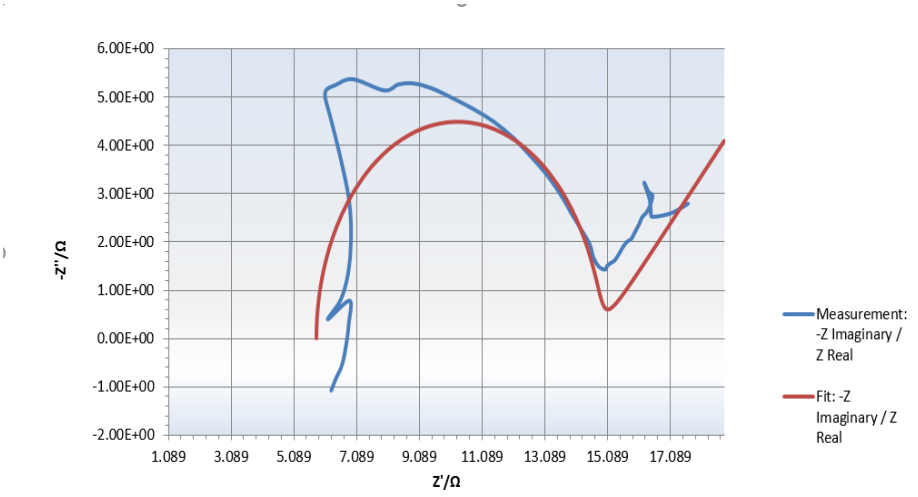

Figure 50: EIS data plot for PANI

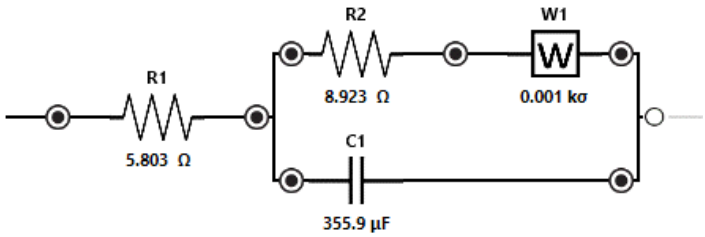

Figure 51: Equivalent circuit modelling for PANI

- ✓ **PANI/GO:**

The EIS data for the PANI/GO electrode, modeled using an equivalent circuit, includes solution resistance (R1 = 6.153 Ω), charge transfer resistance (R2 = 4.438 Ω), double layer capacitance (C1 = 370 µF), and Warburg impedance (W1 = 4 Ω) as shown in (Figure 53). The Nyquist plot (Figure 52) shows the real part of the impedance (Z') on the x-axis and the negative imaginary part of the impedance (-Z") on the y-axis, with the blue line representing measured data and the red line representing fitted data. In the high-frequency region, the plot indicates the dominance of the solution resistance (R1). The mid-frequency range shows a semicircle corresponding to the charge transfer resistance (R2) and double layer capacitance (C1). In the low-frequency region, a linear increase suggests the presence of Warburg impedance (W1), indicating diffusion-controlled processes. The fit between the measured and modeled data is reasonably good, suggesting the appropriateness of the equivalent circuit model. The significant double layer capacitance (C1) indicates a large surface area and good capacitive behavior, while the moderate charge transfers resistance (R2) suggests reasonable efficiency in charge transfer processes. The Warburg impedance (W1) indicates efficient ion diffusion. Overall, the PANI/GO electrode shows promising electrochemical properties for applications requiring efficient charge storage and transfer, although some charge losses are due to internal resistance and the sulfuric acid electrolyte [33,41].

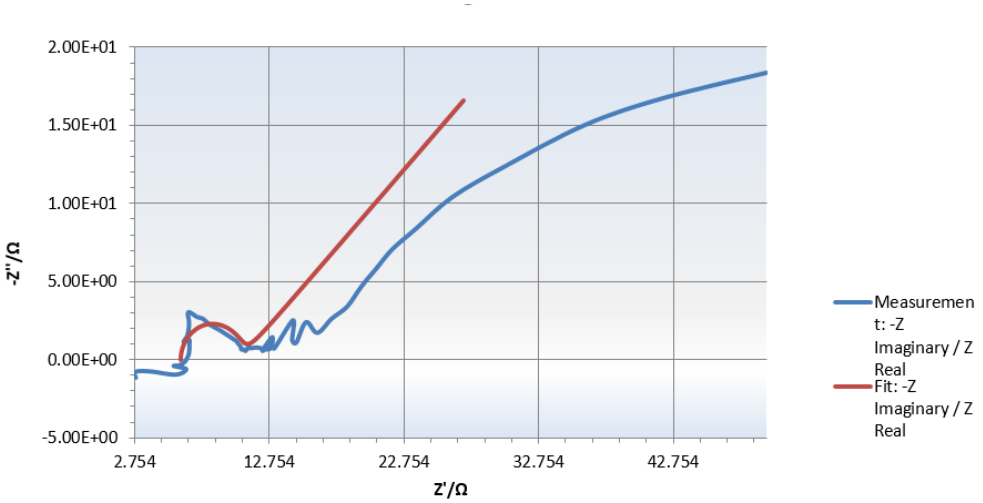

Figure 52:EIS data plot for PANI/GO

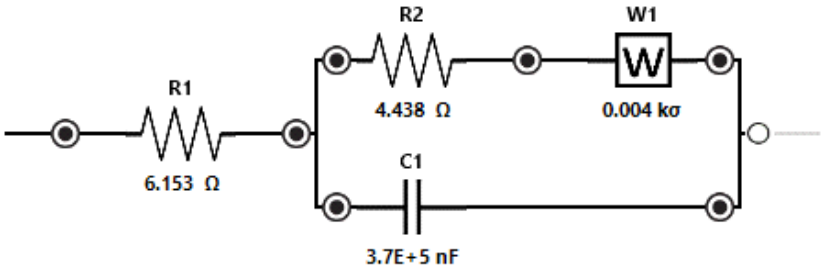

Figure 53:Equivalent circuit modelling for PANI/GO

- ✓ **PANI/ZnO:**

The EIS data for the PANI/ZnO electrode, modeled using an equivalent circuit, includes solution resistance (R1 = 5.892 Ω), charge transfer resistance (R2 = 1.906 Ω), double layer capacitance (C1 = 421.5 µF), and Warburg impedance (W1 = 1 Ω) as shown on (Figure 55). The Nyquist plot (Figure 54) shows the real part of the impedance (Z') on the x-axis and the negative imaginary part of the impedance (-Z'') on the y-axis, with the blue line representing measured data and the red line representing fitted data. In the high-frequency region, the plot indicates the dominance of the solution resistance (R1). The mid-frequency range shows a semicircle corresponding to the charge transfer resistance (R2) and double layer capacitance (C1). In the low-frequency region, a linear increase suggests the presence of Warburg impedance (W1), indicating diffusion-controlled processes. The fit between the measured and modeled data is reasonably good, suggesting the appropriateness of the equivalent circuit model. The significant double layer capacitance (C1) indicates a large surface area and excellent capacitive behavior, while the low charge transfers resistance (R2) suggests efficient charge transfer processes. The Warburg impedance (W1)

indicates efficient ion diffusion. Overall, the PANI/ZnO electrode shows promising electrochemical properties for applications requiring efficient charge storage and transfer, with improved performance over the PANI and PANI/GO electrodes [23,33].

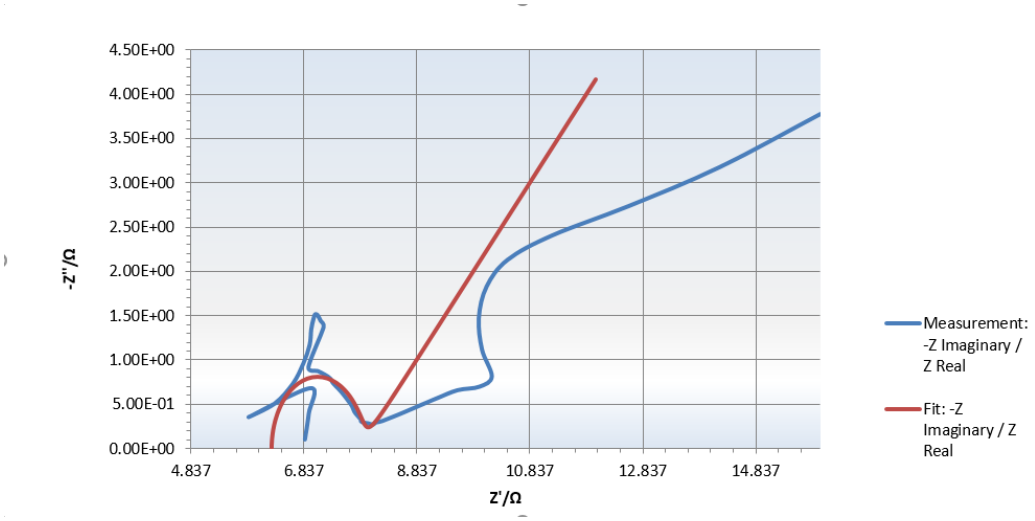

Figure 54:EIS data plot for PANI/ZnO

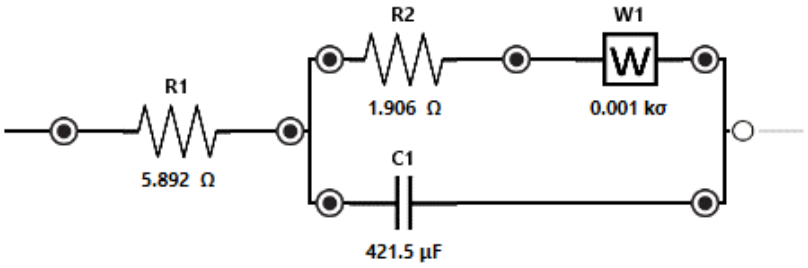

Figure 55:Equivalent circuit modelling for PANI/ZnO

- ✓ **PANI/GO/ZnO:**

The EIS data for the PANI/GO/ZnO electrode, modeled using an equivalent circuit, includes solution resistance (R1 = 7.180 Ω), charge transfer resistance (R2 = 2.946 Ω), double layer capacitance (C1 = 492.7 µF), and Warburg impedance (W1 = 0.87 Ω) as shown on (Figure 57). The Nyquist plot (Figure 56) shows the real part of the impedance (Z') on the x-axis and the negative imaginary part of the impedance (-Z'') on the y-axis, with the blue line representing measured data and the red line representing fitted data. In the high-frequency region, the plot indicates the dominance of the solution resistance (R1). The mid-frequency range shows a semicircle corresponding to the charge transfer resistance (R2) and double layer capacitance (C1).

In the low-frequency region, a linear increase suggests the presence of Warburg impedance (W1), indicating diffusion-controlled processes. The fit between the measured and modelled data is reasonably good, suggesting the appropriateness of the equivalent circuit model. The high double layer capacitance (C1) indicates a large surface area and excellent capacitive behaviour, while the lower charge transfers resistance (R2) compared to the PANI and PANI/GO electrodes suggests improved charge transfer efficiency. The Warburg impedance (W1) indicates efficient ion diffusion. Overall, the PANI/GO/ZnO electrode demonstrates superior electrochemical properties, making it a promising candidate for applications requiring efficient charge storage and transfer [23,33,42].

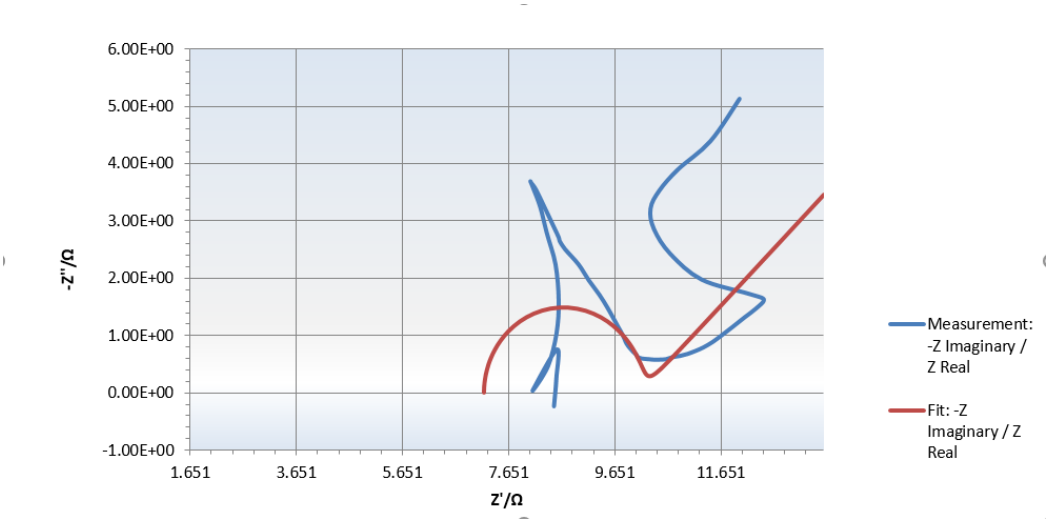

Figure 56:EIS data plot for PANI/GO/ZnO

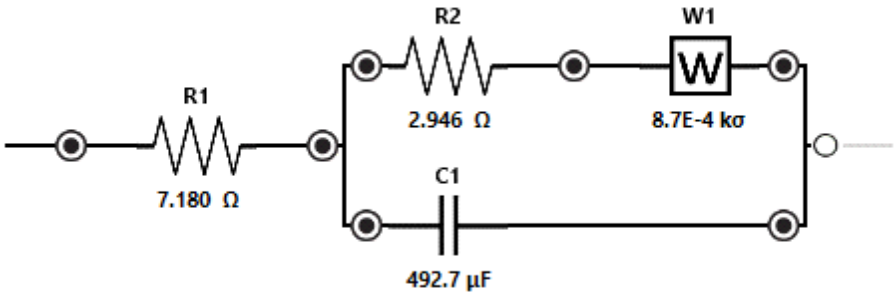

Figure 57:Equivalent circuit modelling for PANI/GO/ZnO

Table 9:EIS Data Summary for Different Electrodes (PANI, PANI/GO, PANI/ZnO, PANI/GO/ZnO)

Electrode	**R1 (Ω)**	**R2 (Ω)**	**C1 (μF)**	**W1 (Ω)**
PANI	5.803	8.923	355.9	1
PANI/GO	6.153	4.438	370	4
PANI/ZnO	5.892	1.906	421.5	1
PANI/GO/ZnO	7.18	2.946	492.7	0.87

The EIS analysis of the PANI, PANI/GO, PANI/ZnO, and PANI/GO/ZnO electrodes reveals significant enhancements in electrochemical performance with the incorporation of graphene oxide (GO) and zinc oxide (ZnO) as shown on table 9. The solution resistance (R1) is relatively similar across all electrodes, indicating comparable ionic conductivity in the electrolyte solutions. PANI/GO exhibits a significantly lower charge transfer resistance (R2) of 4.438 Ω compared to PANI's 8.923 Ω, indicating better charge transfer efficiency due to GO. PANI/ZnO has the lowest R2 at 1.906 Ω, suggesting that zinc incorporation greatly improves charge transfer processes. The PANI/GO/ZnO electrode has an R2 of 2.946 Ω, better than PANI and PANI/GO, but slightly higher than PANI/ZnO, indicating a balanced improvement in charge transfer efficiency. The double layer capacitance (C1) is highest for PANI/GO/ZnO at 492.7 μF, indicating a large surface area and excellent capacitive behaviour. PANI/ZnO also shows high capacitance at 421.5 μF, followed by PANI (355.9 μF) and PANI/GO (370 μF), suggesting that both zinc and the combination of zinc and graphene oxide enhance capacitive behaviour. The Warburg impedance (W1) is lowest for PANI/GO/ZnO (0.87 Ω) and PANI/Zn (1 Ω), indicating efficient ion diffusion, while PANI/GO has a higher W1 (4 Ω). Overall, the PANI/GO/ZnO electrode demonstrates the best electrochemical properties, making it a promising candidate for applications requiring efficient charge storage and transfer.

General Conclusion and perspectives

In this study, we explored the development and characterization of PANI/GO/ZnO composite electrodes for supercapacitors application using electrodeposition techniques. The research focused on optimizing the electrodeposition parameters to enhance the electrochemical performance of the composite electrodes.

Key findings from the electrochemical analyses revealed that:

the PANI/GO/ZnO composite electrodes exhibited significantly improved performance compared to other samples, including PANI, PANI/GO, and PANI/ZnO composites. - - Cyclic voltammetry (CV) showed that PANI/GO/ZnO electrodes achieved higher specific capacitance, indicating superior energy storage capacity.

The galvanostatic charge-discharge (GCD) tests demonstrated better charge-discharge efficiency and stability, while electrochemical impedance spectroscopy (EIS) highlighted reduced internal resistance and enhanced ion transport within the electrodes. The PANI/GO/ZnO electrode allows a charging time of 150.9 s, a discharging time of 209.8 s exhibiting thus an efficiency of 139%, and an energy density of 9.8 Wh/Kg.

Microscopic and structural characterizations using Scanning Electron Microscopy (SEM) and X-Ray Diffraction (XRD) provided detailed insights into the morphology and crystalline structure of the composite electrodes. SEM analysis revealed uniform deposition and well-integrated structures, while XRD confirmed the successful synthesis of the composite materials and the presence of distinct phases of PANI, GO, and ZnO.

The study also found that the electrodeposition parameters, such as current density and deposition time, played a crucial role in determining the electrochemical properties of the electrodes. By optimizing these parameters, we were able to achieve a desirable balance between capacitance, energy density, and stability.

Overall, this research demonstrates that the development of PANI/GO/ZnO composite electrodes through electrodeposition is a promising approach for enhancing the performance of supercapacitors. The findings provide valuable insights for future research and practical applications in the field of energy storage. The present work consists on a preliminary study and by fine-tuning the electrodeposition process (by using other sources to provide ZnO and pure GO in order to enhance the efficiency of the electrodes), it is possible to create high-performance supercapacitors that are both efficient and durable, thereby contributing to advancements in energy storage technologies.

Bibliography

[1] Sahani S, Mahajan H, Han SS. Unveiling the hybrid era: Advancement in electrode materials for the high-performance supercapacitor: A comprehensive review. Journal of Energy Storage 2024;90:111808. https://doi.org/10.1016/j.est.2024.111808.

[2] George L. Facile electrochemical synthesis of rGO/PANI/ZnO heterostructure for energy storage applications. Materials Today: Proceedings 2023.

https://doi.org/10.1016/j.matpr.2023.01.417.

[3] Shah SS, Niaz F, Ehsan MA, Das HT, Younas M, Khan AS, et al. Advanced strategies in electrode engineering and nanomaterial modifications for supercapacitor performance enhancement: A comprehensive review. Journal of Energy Storage 2024;79:110152. https://doi.org/10.1016/j.est.2023.110152.

[4] Conway BE. Electrochemical Supercapacitors: Scientific Fundamentals and Technological Applications. Springer Science & Business Media; 2013.

[5] Wang Y, Song Y, Xia Y. Electrochemical capacitors: mechanism, materials, systems, characterization and applications. Chemical Society Reviews 2016;45:5925–50. https://doi.org/10.1039/C5CS00580A.

[6] Keum K, Kim J, Hong S, Son J, Lee S-S, Ha J. Flexible/Stretchable Supercapacitors with Novel Functionality for Wearable Electronics. Advanced Materials (Deerfield Beach, Fla) 2020;32:e2002180. https://doi.org/10.1002/adma.202002180.

[7] Electrochemical investigation of ionic liquid-derived porous carbon materials for supercapacitors: pseudocapacitance versus electrical double layer | Semantic Scholar n.d.

[8] Ehsani A, Moftakhar M. Enhanced electrochemical pseudocapacitance performance of poly tyramine composite on the surface of polyethylene glycol modified electrode. Plastics, Rubber and Composites: Macromolecular Engineering 2023.

[9] Chen S-M, Ramachandran R, Mani V, Saraswathi R. Recent Advancements in Electrode Materials for the Highperformance Electrochemical Supercapacitors: A Review. International Journal of Electrochemical Science 2014;9:4072–85. https://doi.org/10.1016/S1452-3981(23)08076-8.

[10] He X, Zhang X. A comprehensive review of supercapacitors: Properties, electrodes, electrolytes and thermal management systems based on phase change materials. Journal of Energy Storage 2022;56:106023. https://doi.org/10.1016/j.est.2022.106023.

[11] Islam S, Lakshmi GBVS, Siddiqui AM, Husain M, Zulfequar M. Synthesis, Electrical Conductivity, and Dielectric Behavior of Polyaniline/V_2O_5 Composites. International Journal of Polymer Science 2013;2013:e307525. https://doi.org/10.1155/2013/307525.

[12] Synthesis of polyaniline by chemical oxidative polymerization and characteristic of conductivity and reflection for various strong acid dopants - IOPscience n.d. https://iopscience.iop.org/article/10.1088/1742-6596/1442/1/012003/meta (accessed May 6, 2024).

[13] Research Progress on Applications of Polyaniline (PANI) for Electrochemical Energy Storage and Conversion n.d. http://ouci.dntb.gov.ua/en/works/96OrXkx7/ (accessed May 5, 2024).

[14] Polyaniline for Smart Textile Applications n.d.

[15] Kurnakov Institute of General and Inorganic Chemistry. Russian Academy of Sciences, Fatyushina EV, Buslaeva EYu, Kurnakov Institute of General and Inorganic Chemistry. Russian Academy of Sciences. REDUCTION OF GRAPHENE OXIDE BY SUPERCRITICAL ISOPROPANOL: DEFINITION OF ACETONE IN THE COMPOSITION OF THE MULTICOMPONENT MIXTURE BY GC-MS METHOD. Radioelectronics. Nanosystems. Information Technologies, vol. 11, 2019, p. 307–14. https://doi.org/10.17725/rensit.2019.11.307.

[16] Boudjellal A, Khimeche K, Trache D, Hafsaoui S, Razali M. Preparation and characterization of hybrid fibers based on graphene oxide-wood flour for advanced applications. Materials Today: Proceedings 2021;49. https://doi.org/10.1016/j.matpr.2021.05.703.

[17] Anwar A, Chang T-P, Chen C-T. Graphene oxide synthesis using a top–down approach and discrete characterization techniques: a holistic review. Carbon Lett 2022;32:1–38. https://doi.org/10.1007/s42823-021-00272-z.

[18] Liu L, Lin X-X, Zou S-Y, Wang A-J, Chen J-R, Feng J-J. One-pot wet-chemical synthesis of PtPd@Pt nanocrystals supported on reduced graphene oxide with highly electrocatalytic performance for ethylene glycol oxidation. Electrochimica Acta 2016;187:576–83. https://doi.org/10.1016/j.electacta.2015.11.089.

[19] Yakovlev AV, Yakovleva EV, Tseluikin VN, Krasnov VV, Mostovoy AS, Rakhmetulina LA, et al. Electrochemical Synthesis of Multilayer Graphene Oxide by Anodic Oxidation of Disperse Graphite. Russ J Electrochem 2019;55:1196–202. https://doi.org/10.1134/S102319351912019X.

[20] Sengunthar P, Patel S, Thankachen N, Joshi US, Pandya RJ. Controlled Synthesis of Reduced Graphene Oxide Sheets on Large Scale Using Thermal Exfoliation. ECS Trans 2022;107:19943–8. https://doi.org/10.1149/10701.19943ecst.

[21] Fundamental Properties and Applications of Zinc Oxide Nanoparticles. Nanografi Nano Technology n.d. https://nanografi.com/blog/fundamental-properties-and-applications-of-zinc-oxide-nanoparticles/ (accessed May 6, 2024).

[22] Pushpalatha C, Suresh J, Gayathri VS, Sowmya SV, Augustine D, Alamoudi A, et al. Zinc Oxide Nanoparticles: A Review on Its Applications in Dentistry. Front Bioeng Biotechnol 2022;10. https://doi.org/10.3389/fbioe.2022.917990.

[23] Rahal H, Kihal R, Affoune AM, Ghers M, Djazi F. Electrodeposition and characterization of ZnO thin films using sodium thiosulfate as an additive for photovoltaic solar cells*. J Semicond 2017;38:053002. https://doi.org/10.1088/1674-4926/38/5/053002.

[24] Stain G. Nanoparticle Synthesis with Co Precipitation. Research & Reviews: Journal of Pharmaceutics and Nanotechnology 2022;10:11–2.

[25] Guglielmi M. Sol-gel science: Edited by C. Jeffrey Brinker and George Scherer Academic Press Inc., London 1990. 912 pp., $139. Materials Chemistry and Physics 1990;26:211–2. https://doi.org/10.1016/0254-0584(90)90039-D.

[26] Fathima F, Mani RJ, Kathiresan S, Manimala K, Hossain A. Enhanced Antifungal Activity of Pure and Iron-Doped ZnO Nanoparticles Prepared in the Absence of Reducing Agents. Journal of Inorganic and Organometallic Polymers and Materials 2020;30:1–9. https://doi.org/10.1007/s10904-019-01400-z.

[27] Berrueta A, San Martín I, Hernández A, Ursúa A, Sanchis P. Electro-thermal modelling of a supercapacitor and experimental validation. Journal of Power Sources 2014;259:154–65. https://doi.org/10.1016/j.jpowsour.2014.02.089.

[28] Carbon-Based Supercapacitors Produced by Activation of Graphene | Science n.d. https://www.science.org/doi/10.1126/science.1200770 (accessed May 6, 2024).

[29] Ajina A, Isa D. Capacitance and equivalent series resistance (ESR) optimization using the Taguchi technique for EDLC's. 2010 International Conference on Electronic Devices, Systems and Applications 2010:335–9. https://doi.org/10.1109/ICEDSA.2010.5503046.

[30] Grama A, Petreus D, Borza P, Grama L. Experimental determination of Equivalent Series Resistance of a supercapacitor. 2009 32nd International Spring Seminar on Electronics Technology 2009:1–4. https://doi.org/10.1109/ISSE.2009.5207057.

[31] Electrochemical Methods: Fundamentals and Applications, 2nd Edition | Wiley. WileyCom n.d. https://www.wiley.com/en-us/Electrochemical+Methods%3A+Fundamentals+and+Applications%2C+2nd+Edition-p-9780471043720 (accessed July 2, 2024).

[32] Parsons R. Cyclic voltammetry and the frontiers of electrochemistry: M. Noel and K.I. Vasu. Aspect, London, 1990, xxiv + 702 pp., £25.00. Journal of Electroanalytical Chemistry and Interfacial Electrochemistry 1991;305:164–6. https://doi.org/10.1016/0022-0728(91)85213-9.

[33] Macdonald JR, Johnson WB. Fundamentals of Impedance Spectroscopy. Impedance Spectroscopy, John Wiley & Sons, Ltd; 2018, p. 1–20. https://doi.org/10.1002/9781119381860.ch1.

[34] Fletcher S, Black VJ, Kirkpatrick I. A universal equivalent circuit for carbon-based supercapacitors. J Solid State Electrochem 2014;18:1377–87. https://doi.org/10.1007/s10008-013-2328-4.

[35] Arumugam C, Kandasamy SK, Kumaravel Subramaniam T. Enhancement of the Carbon Content and Electrochemical Performance by Decorating Zinc Oxide Over Graphene Oxide/Polyaniline Composite. Journal of Electrochemical Energy Conversion and Storage 2023;20. https://doi.org/10.1115/1.4056531.

[36] Beygisangchin M, Abdul Rashid S, Shafie S, Sadrolhosseini AR, Lim HN. Preparations, Properties, and Applications of Polyaniline and Polyaniline Thin Films—A Review. Polymers 2021;13:2003. https://doi.org/10.3390/polym13122003.

[37] Chen Y. A review of polyaniline based materials as anodes for lithiumion batteries. IOP Conference Series: Materials Science and Engineering 2019;677:022115. https://doi.org/10.1088/1757-899X/677/2/022115.

[38] Tian Y, Wang Y, Wang Y, Ma L, Gao X. Utilizing polyaniline to decorate graphene and its effect on the electrochemical properties of polyaniline/graphene electrode composite. Mater Res Express 2019;6:105614. https://doi.org/10.1088/2053-1591/ab3bf4.

[39] Bibi A, Shakoor A, Raffi M, Hina M, Niaz NA, Fatima SA, et al. Exploring the potential of polyaniline-calcium titanate (PANI-CaTiO3) nanocomposites in supercapacitors: Synthesis and electrochemical investigation. Journal of Energy Storage 2024;78:110321. https://doi.org/10.1016/j.est.2023.110321.

[40] Said MBH, Charradi K, Ahmed Z, Cachet H, Debiemme-Chouvy C, Alsulami Q, et al. Synthesis and characterization of cellulose hydrogel/graphene oxide/polyaniline composite for high-performing supercapacitors. International Journal of Energy Research 2022;46:13844. https://doi.org/10.1002/er.8102.

[41] Wang Y, Wang Y, Tian Y, Ma L, Wang C, Gao X. Fabrication and Characterization of Graphene Oxide/Polyaniline Electrode Composite for High Performance Supercapacitors. ECS J Solid State Sci Technol 2019;8:M103. https://doi.org/10.1149/2.0231910jss.

[42] Lee KS, Park CW, Lee SJ, Kim J-D. Hierarchical zinc oxide/graphene oxide composites for energy storage devices. Journal of Alloys and Compounds 2018;739:522–8. https://doi.org/10.1016/j.jallcom.2017.12.248.

[43] Chee WK, Lim HN, Huang NM. Electrochemical properties of free-standing polypyrrole/graphene oxide/zinc oxide flexible supercapacitor. International Journal of Energy Research 2015;39:111–9. https://doi.org/10.1002/er.3225.

[44] Gul H, Shah A-HA, Krewer U, Bilal S. Study on Direct Synthesis of Energy Efficient Multifunctional Polyaniline–Graphene Oxide Nanocomposite and Its Application in Aqueous Symmetric Supercapacitor Devices. Nanomaterials 2020;10:118. https://doi.org/10.3390/nano10010118.

[45] Altıncı OC, Körbahti BK. Graphene oxide-polyaniline conducting composite film deposited on platinum-iridium electrode by electrochemical polymerization of aniline: Synthesis and environmental electrochemistry application. Applied Surface Science Advances 2022;7:100212. https://doi.org/10.1016/j.apsadv.2022.100212.

[46] Shoaie N, Daneshpour M, Azimzadeh M, Mahshid S, Khoshfetrat SM, Jahanpeyma F, et al. Electrochemical sensors and biosensors based on the use of polyaniline and its nanocomposites: a review on recent advances. Microchimica Acta 2019;186. https://doi.org/10.1007/s00604-019-3588-1.

[47] M. Jayalakshmi, K. Balasubramanian, 2008, Simple Capacitors to Supercapacitors - An Overview, Int. J. Electrochem. Sci, 3, 1196 – 1217.

[48] B. E. Conway, Electrochemical Supercapacitors Scientific Fundamentals and Technological Applications, New York: Business Media 1999. ISBN 978-1-4757-3060-9.

[48] A.Yu, V.Chabot, J.Zhang, Electrochemical Supercapacitors for Energy Storage and Delivery Fundamentals and Applications, Boca Raton: Taylor & Francis Group, LLC 2013. ISBN 13: 978-1-4398-6990-1, Z. Iro, et al.

[50] A Brief Review on Electrode Materials for Supercapacitor, International Journal of Electrochemical Science, 11, (2016), 10628 – 10643.

[51] B. E. Conway, Electrochemical Supercapacitors Scientific Fundamentals and Technological Applications, New York: Business Media 1999. ISBN 978-1-4757-3060-9.

[52] P. Sharma, T.S. Bhatti, A review on electrochemical double-layer capacitors, Energy Conversion and Management, 51, (2010), 2901–2912.

[53] A.Yu, V.Chabot, J.Zhang , Electrochemical Supercapacitors for Energy Storage and Delivery Fundamentals and Applications , Boca Raton: Taylor & Francis Group, LLC 2013.ISBN 13: 978- 1-4398-6990-1.

[54] Z. Qi et al, A Facile and Template-Free One-Pot Synthesis of Mn3O4 Nanostructures as Electrochemical Supercapacitors, Nano-Micro Lett, 8, (2016),165–173.

[55] K. Akhtar Scanning Electron Microscopy: Principle and Applications in Nanomaterials Characterization, Handbook of Materials Characterization, Springer,2012.

[56] P. Echlin, Handbook of Sample Preparation for Scanning Electron Microscopy and X-Ray Microanalysis, Springer, 2009.ISBN 978-0-387-85730-5.

[57] F. Serna, La diffraction des rayons X : une technique puissante pour résoudre certains problèmes industriels et technologiques, Chimie Nouvelle, 116, (2014), 1-12.

Annex

Real-time Monitoring and Data Treatment Using PSTrace Software

Introduction

For the real-time monitoring and data treatment of the electrochemical experiments, PSTrace software was utilized. This software is designed to work seamlessly with various electrochemical instruments, providing advanced data acquisition and analysis capabilities.

PSTrace Software:

- Version: 5.10.5604

- Developer:PalmSens BV

- Website: PSTrace - PalmSens

PSTrace is a powerful tool for electrochemical data acquisition and analysis. It supports a wide range of electrochemical techniques and is compatible with various potentiostats and galvanostats.

Features and Capabilities

- Real-time Data Monitoring: PSTrace allows for real-time visualization of electrochemical data during experiments, enabling immediate observation of the electrochemical behavior of the samples.

- Data Treatment: The software provides advanced tools for data analysis, including baseline correction, peak analysis, and integration.

- Multiple Technique Support: Supports various electrochemical techniques such as cyclic voltammetry (CV), chronoamperometry, and electrochemical impedance spectroscopy (EIS).

- Graphical Representation: Generates detailed graphs and plots for a comprehensive understanding of the electrochemical processes.

- Export Options: Data can be exported in multiple formats for further analysis or reporting.

Application in This Study

In this study, PSTrace was employed to monitor the real-time electrodeposition process and analyze the resulting data. The software facilitated:

- Cyclic Voltammetry (CV) Analysis: Real-time monitoring of CV curves during the electrodeposition of PANI, GO, and ZnO.

- Peak Identification: Accurate identification and analysis of redox peaks corresponding to the different stages of electrodeposition.

- Data Export: Exporting the CV data for further analysis and incorporation into the research findings.

Steps for Using PSTrace

1. Setup:

- Connect the electrochemical workstation to the computer and launch PSTrace.

- Configure the software settings to match the experimental parameters (e.g., scan rate, potential range).

2. Data Acquisition:

- Begin the electrochemical experiment, and monitor the real-time data using PSTrace.

- Adjust the experimental conditions if necessary, based on the real-time feedback.

3. Data Analysis:

- Use the software's built-in tools to analyze the recorded data.

- Perform baseline correction, peak integration, and other relevant data treatments.

4. Data Export:

- Export the treated data in the desired format for inclusion in the research report.

Figure 58: Pstrace software and the potentiosta